UC Riverside
UC Riverside Electronic Theses and Dissertations

Title

Re-Investigation of Reaction Kinetics and Charge Transfer Phenomena in Watersplitting Process by Cocatalyst-Loaded GaNZnO Particulate Photocatalytic Systems

Permalink

Author

Jiang, Yibo

Publication Date

2017

Peer reviewed|Thesis/dissertation

UNIVERSITY OF CALIFORNIA
RIVERSIDE

Re-Investigation of Reaction Kinetics and Charge Transfer Phenomena in Water Splitting
Process by Cocatalyst-Loaded GaNZnO Particulate Photocatalytic Systems

A Thesis submitted in partial satisfaction
of the requirements for the degree of

Master of Science

in

Chemical and Environmental Engineering

by

Yibo Jiang

June 2017

Thesis Committee:

      Dr. Phillip Christopher, Chairperson
      Dr. Juchen Guo
      Dr. Jinyong Liu

The Thesis of Yibo Jiang is approved:

_____

_____

_____
                                        Committee Chairperson

University of California, Riverside

ACKNOWLEDGEMENTS

First and foremost, I genuinely appreciate the lab group I have been working for. I always feel honored to get a chance to work with many amazing people. I am grateful to have Dr. Phillip Christopher as my adviser who guided through academic difficulties with great patience and support. I also want to express my acknowledgement to Dr. Jinyong Liu and Dr. Juchen Guo for their willingness to serve on my defense committee and instructions given to me over the years.

I am always thankful for my awesome lab colleagues who spent up and down times with me and granted me tremendous support. Thank you: John, Matt, Talin, Leo, Sergei, Christian, Kun, Chithra, Glen, and many more good people whom I met with great fortune in Riverside.

Here I also want to thank several great researchers from outside our lab, but still have valuable contribution for my projects, they are Dr. Bozhilov and Dr. Mecklenburg for microscopy assistance; Dr. Rao and Duncan for the joint venture from ME department.

DEDICATIONS

This thesis is dedicated to my family members, including: Grandma, Dad, and Mom for your eternal support and love granted to my life.

ABSTRACT OF THE THESIS

Re-Investigation of Reaction Kinetics and Charge Transfer Phenomena in Water Splitting
Process by Cocatalyst-Loaded GaNZnO Particulate Photocatalytic Systems

by

Yibo Jiang

Master of Science, Graduate Program in Chemical and Environmental Engineering
University of California, Riverside, June 2017
Dr. Phillip Christopher, Chairperson

The present work employs a variety of approaches and techniques to explore the photocatalytic water splitting phenomena of a well-known particulate photocatalyst—Gallium Zinc Oxynitride (GaNZnO) from two aspects: reaction kinetics and charge transfer phenomena.

Cocatalyst loading onto n-type semiconductors has been proven to be a highly effective approach to promote the activity of catalysts in photocatalytic processes. Water splitting by particulate photocatalyst (PPC) systems, as a phenomenon, are usually studied via a macroscopic approach developed for Photoelectrochemical Cell (PEC) systems. However, the macroscopic nature of the PEC systems may have overlooked the subtle while intrinsic aspects of the PPC systems due to challenges in characterization techniques and biased views in describing such microscopic systems. Thus, a fundamental re-investigation of water splitting process by cocatalyst-loaded PPC systems

via exploring rate-limiting reaction kinetics and charge transfer phenomena could provide more insights for the study and the improvement of PPC systems in water splitting.

The water splitting kinetics of GaNZnO PPC systems were explored through overall water splitting (OWS) and half-reaction experiments: hydrogen evolution reactions (HER) and oxygen evolution reactions (OER). The photoelectron tracing experiment was developed specifically to clarify the charge transfer direction on GaNZnO surface. Our kinetics results demonstrated up to 6-fold HER rate by RhO_x/GaNZnO system with the presence of sacrificial reagent. The water splitting rates of other metal oxide cocatalysts also increased by at least 30% by $RhCrO_x$ cocatalyst, which revealed the oxidation half reaction. The varied water splitting performance of GaNZnO improved by metal oxide loading reveals that water splitting is not only just limited by reduction half reaction as previously claimed.

In addition, various characterization techniques, such as: UV-VIS, XRD, HRTEM, Dark-field STEM and EDS were applied to gain more knowledge of the PPC system before and after reactions. From the kinetic experiments, we observed unusual rate trends which contradict or deviate from results predicted by PEC models. Further investigation indicates that those unusual behaviors were explained by an opposite charge transfer direction previously proposed by PEC models.

Table of Contents

List of Figures

List of Tables

Chapter 1: Background and Introduction

1.1 Critical Role of Hydrogen in Our Society

The rapid growth of human population demands tremendous energy and industrial products to consume, such that our society can be further developed and advanced. Conservative prediction estimates that the energy consumption rate (currently approximately 14 TW[1]) of human society will be doubled by 2050[2] in order to maintain the current standard of living, and foster further societal developments.

Hydrogen, as the most plentiful element in universe, participates in the formation of numerous compounds. In addition, molecular hydrogen (H_2) possesses advantageous properties (such as high energy content, non-toxicity, and zero emission) that turns hydrogen into an excellent candidate of energy carrier[3]. Therefore, hydrogen has seen numerous applications as a fuel or as a feedstock for important industrial processes (Figure 1.1).

Figure 1.1 Pyramid diagram showing sources and applications of hydrogen
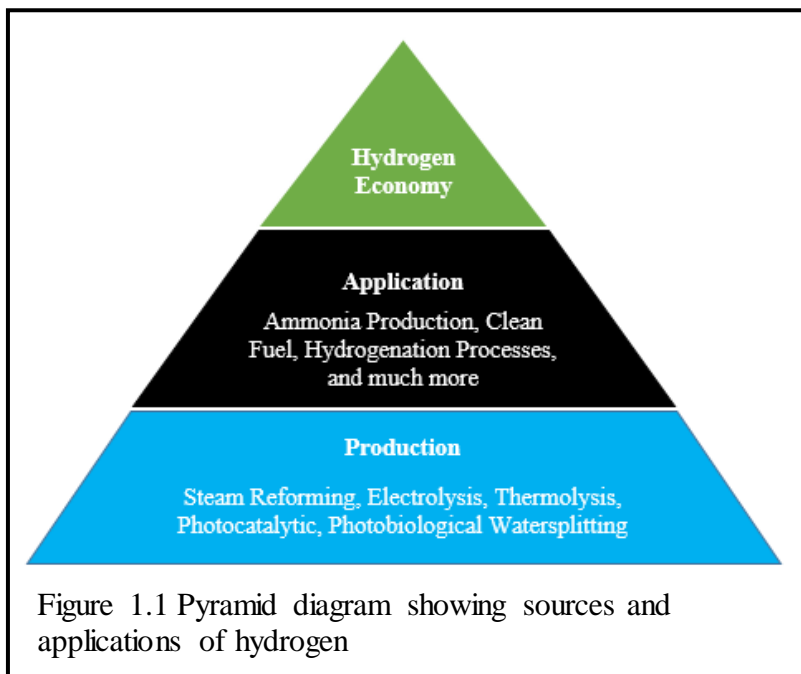
1.1.1 Application as a Clean Energy Carrier

As mentioned above, the unique chemical and physical properties enable hydrogen to potentially serve as a clean fuel for human society. The bond energy stored in molecular hydrogen can be released through ignition inside an internal combustion engine (ICE)[3] or electrochemical redox reactions inside a hydrogen fuel cell (HFC), following the same overall reaction[4].

$$2H_2 + O_2 \rightarrow 2H_2O \qquad \Delta G = -229 \text{ kJ/mol} \qquad \text{Eq. 1.1}$$
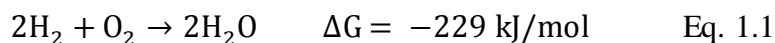
The only emitted chemical species is water, which makes the process environmentally friendly and thermodynamically efficient[4]. Currently the usage of hydrogen as a fuel is still dwarfed by fossil fuel consumption[5], yet it is foreseeable that the exponential growth of hydrogen fuel supply will be enabled by production technology innovation and infrastructure development.

1.1.2 Feedstock for Important Chemical Processes

The famous Baber-Bosch Process synthesizes ammonia[6] which is a critical compound for modern agriculture and industrial production of other chemicals.

$$3H_2 + N_2 \rightarrow 2NH_3 \hspace{4cm} Eq.\ 1.2$$

Globally 176 million metric tons of ammonia was synthesized via this pathway in 2014[6], achieved by massive hydrogen consumed as one of the two reactants. The steady increase of ammonia production since 1946[6] will demand more sustainable hydrogen supply in future in order to increase the agricultural production for the growing global population.

Molecular hydrogen is widely used in various hydrogenation processes. Petroleum industry apply hydrocracking (Figure 1.2) to decompose oil residues into
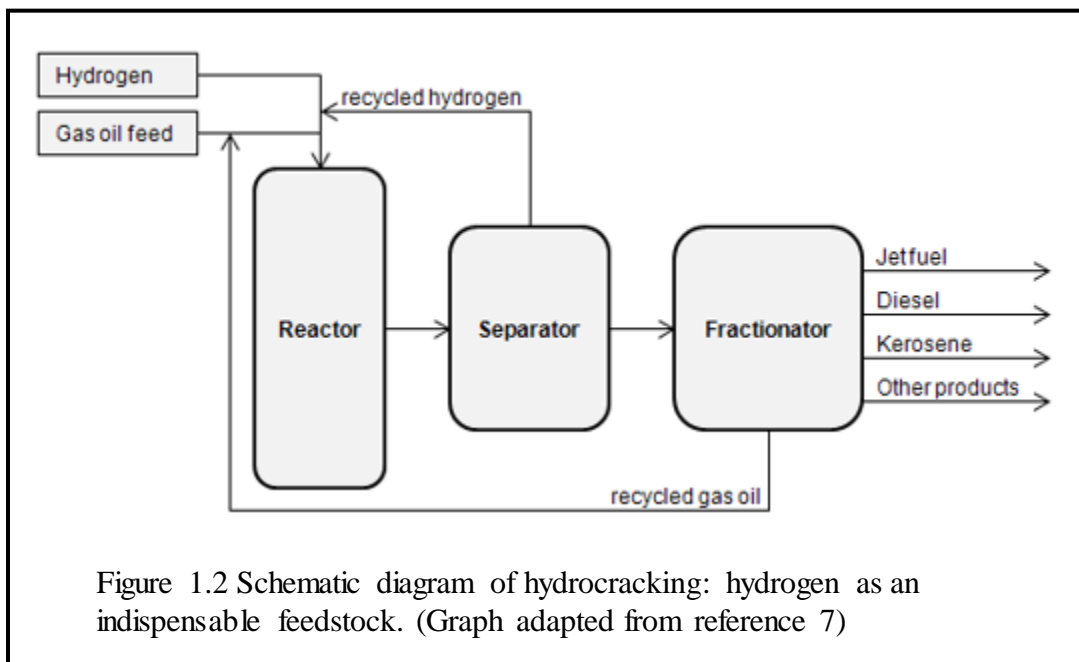
Figure 1.2 Schematic diagram of hydrocracking: hydrogen as an indispensable feedstock. (Graph adapted from reference 7)

useable fuels, such as diesel, kerosene and gasoline, which increases the efficiency of oil refining plants, as well as serves as an significant source of valuable petroleum products[7].

Food industry also utilizes hydrogenation process to saturate vegetable oil and fats, improving the taste and shelf life of the processed food. One well-known type of the hydrogenated fats is called trans-fat added to coffee creamer, crackers, and other snacks[8].

1.1.3 Pillar of Hydrogen Economy

The critical and wide applications of hydrogen, especially as a clean and renewable energy carrier, has led to the conceptualization of the Hydrogen Economy since 1970s[9]. Yet this concept has not been materialized due to various technical difficulties, notably the lack of an efficient, sustainable, and environmentally friendly hydrogen supply system. Therefore harvesting massive energy from sustainable sources has become an increasingly urgent challenge for scientists and engineers. Among the candidates for renewable energy sources, solar energy holds the greatest promise. The Sun irradiates 23000 TW of utilizable solar energy, outnumbering the sum of all other renewable energy sources combined[5]. Thus solar energy has the potential to meet the increased energy demand in an environmentally friendly way. However, harvesting and storing solar energy is not without complications.

1.2 Hydrogen Production via Water splitting

1.2.1 Overview of Water Splitting Concept

Water splitting refers to a process through which water molecules are split into respective elements—oxygen and hydrogen. The overall reaction is described by equation 1.3 below.

$$2H_2O \rightarrow 2H_2 + O_2 \qquad\qquad \text{Eq. 1.3}$$

As the reverse reaction of hydrogen fuel process[4], water splitting is energy-intensive, requiring a minimum Gibbs free energy change of + 229 kJ/mol or 1.23 V overpotential in electrolysis[4]. Nevertheless, this process remains highly attractive, and has great potential to supply massive, sustainable and clean hydrogen[1]; since water is not only recyclable through the hydrogen cycle[10], but also is very high in hydrogen content. Every one cubic meter of water contains 111 kg of hydrogen, compared to 71 kg of hydrogen per every one cubic meter liquid hydrogen[3].

1.2.2 Water Splitting in Nature

In nature plants have been utilizing solar energy as a driving force to initiate the water splitting process via photosystem II (PSII) where water molecules are decomposed into protons, oxygen, and electrons[11]:

$$2H_2O \rightarrow 4H^+ + O_2 + 4e^- \qquad\qquad \text{Eq. 1.4}$$

Inside PSII (figure 1.3) electrons of Chlorophyll molecules are excited by the incident photons, and travel to the primary electron acceptor, which leaves electron vacancies behind. The vacancies are then replenished by taking electrons from water molecules, causing water to be split. Molecular oxygen is released during the process,

while protons and electrons are transported to other enzymes, and participate in the synthesis of energy carriers and carbohydrates[12].

Annotations:

(1) Photosystem II

(2) Chlorophyll molecule

(3) Primary electron acceptor

Figure 1.3 Schematic diagram of water splitting process inside PSII. (Graph adapted from reference 11 and 12)
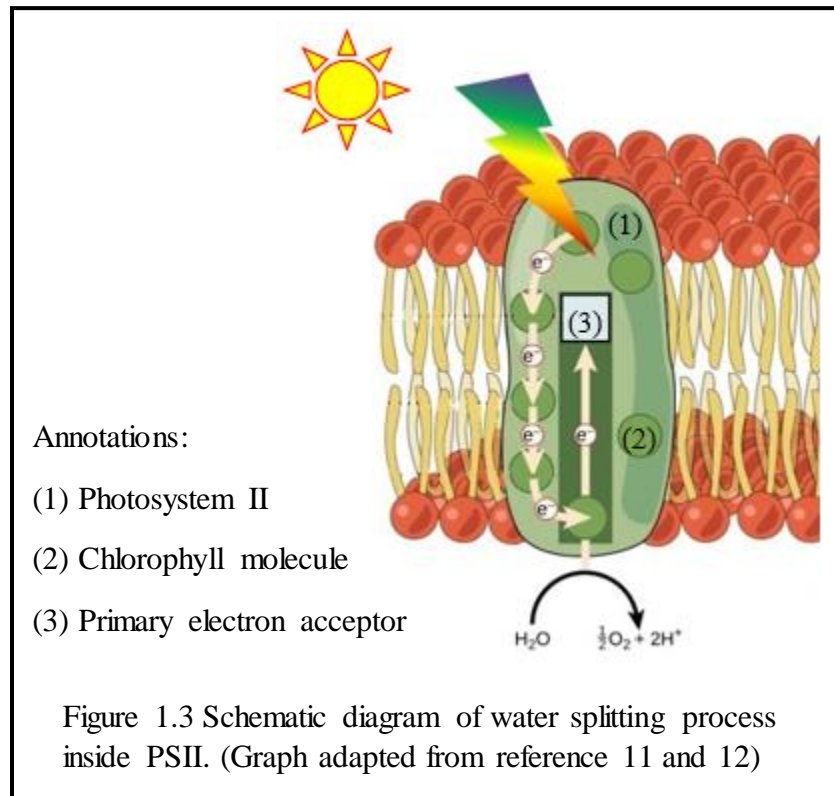
Even though photosynthesis in nature hardly yield molecular hydrogen as product, the water splitting step inspired various artificial water splitting systems utilizing solar energy[1,13,14].

1.2.3 Artificial Water Splitting

Despite that the current hydrogen production (approximately 95% of hydrogen produced annually) is dominated by the carbon-emitting processes, e.g. Steam Methane Reforming (SMR)[15]; artificial water splitting has been studied since 1800[16] via electrolysis and since the late 1960s[17] by photoelectrochemical cells (PEC).

Electrochemical reactions share the same fundamental principle of charge transfer depicted in figure 1.4. The reduction and oxidation of a species is dictated by the relative energy levels of the electrodes and the species in solution. When an electron is at a relatively high energy level (i.e. more negative potential), electron can migrate to the vacant molecular orbital (MO) of the adsorbed species, and drives the reduction reaction. When the energy level of the electrode is lower than that of the occupied MO of the adsorbed species, the species loses electrons to the electrode, driving the oxidation reaction[18]. In other words, the reduction or oxidation of a species can be achieved by a relatively negative or positive electrode potential.

Figure 1.4 Schematic diagram of charge (electron) transfer during reduction (a) and oxidation (b) of electrochemical reactions. (Graph adapted from reference 18)
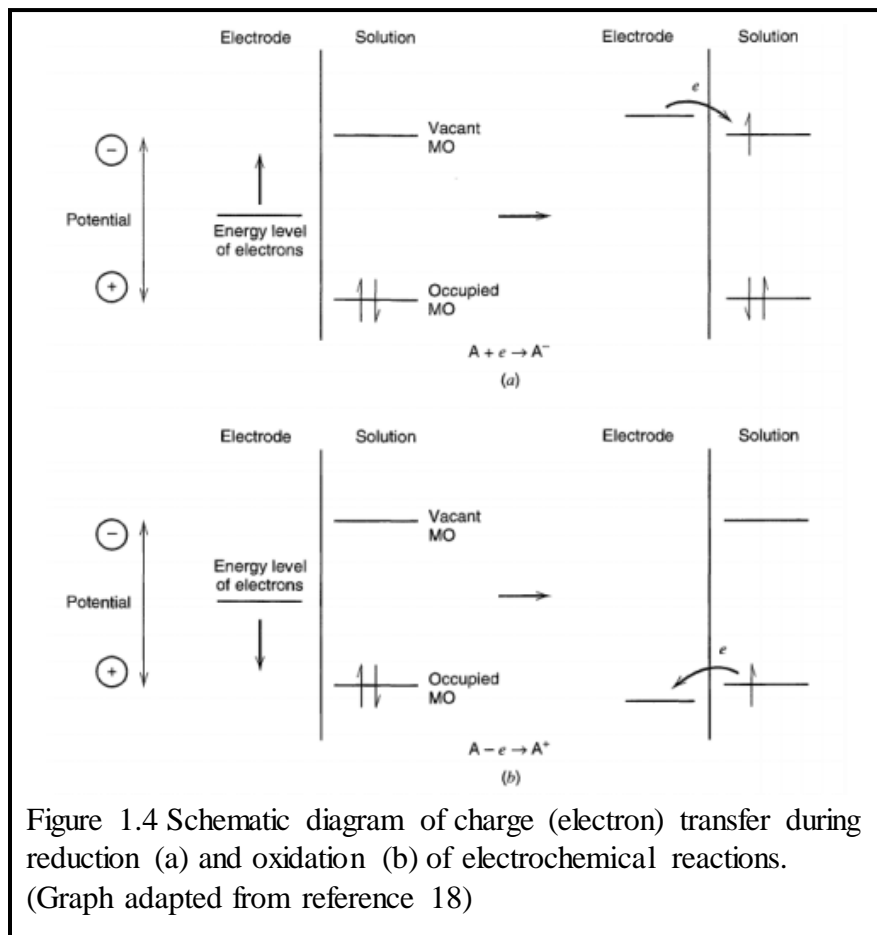
As for overall water splitting (Eq. 1.5), water is both oxidized (Eq. 1.6) and reduced (Eq. 1.7) via the following (photo)electrochemical reactions[1,19]:

Overall reaction: $H_2O \rightarrow H_2 + \frac{1}{2}O_2$ Eq. 1.5

At (photo)anode: $H_2O\ (+2h^+) \rightarrow 2H^+ + \frac{1}{2}O_2 + 2e^-$ Eq. 1.6

At (photo)cathode: $2H^+ + 2e^- \rightarrow H_2$ Eq. 1.7
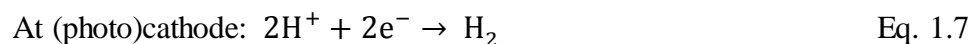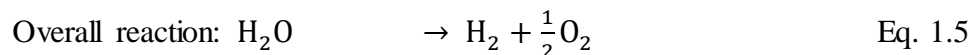
The abovementioned equations are valid for water splitting at neutral or acidic pH. At basic pH, the reduction of water occurs at cathode, releasing hydrogen; while the oxidation of hydroxyl occurs at anode, releasing oxygen[16,19].

At (photo)anode: $2OH^- (+2h^+) \rightarrow H_2O + \frac{1}{2}O_2 + 2e^-$ Eq. 1.8

At (photo)cathode: $2H_2O + 2e^- \rightarrow H_2 + 2OH^-$ Eq. 1.9
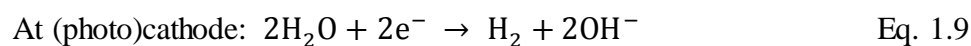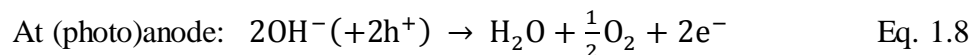
1.3 Configuration of Heterogeneous Photocatalytic Water splitting Systems

Artificial water splitting could be achieved through two main-stream configurations (figure 1.5) of Photocatalytic water splitting systems, namely: photoelectrochemical cells (PEC)[20] and particulate photocatalysts (PPC)[1].
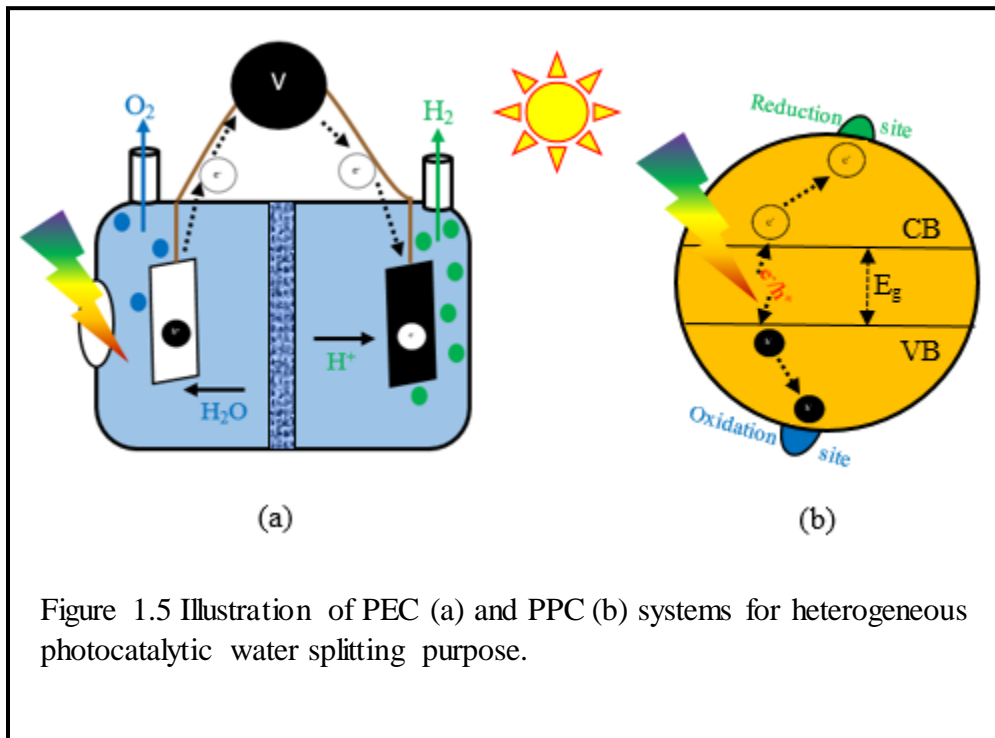
Figure 1.5 Illustration of PEC (a) and PPC (b) systems for heterogeneous photocatalytic water splitting purpose.

The two systems share similarities; while each one possesses distinctive properties, for instance, the contact type between the electrodes. The systems will be introduced in the following sections with more details. The present project emphasizes on the PPC systems.

1.3.1 Macroscopic electrodes: Photoelectrochemical Cells

The work on the PEC configuration (figure 1.5 a) was pioneered by Boddy in 1968[17] and by Fujishima & Honda in 1972[21]. This type of cells is nearly identical to a typical electrolysis cell, which consists of an anode, a cathode and an optional bias source to provide additional overpotential if needed[17,21]. In a common setup, an n-type light-absorber/photocatalyst serves as a photoanode, while a p-type material or a metal serves as (photo)cathode[14,23].

During the photocatalytic reaction, electrons generated by the anode photocatalyst migrate to cathode via external circuit; while holes remain on the photocatalyst (as anode)[22,23]. As a result, hydrogen evolution and oxygen evolution from the cathode and anode surfaces could be observed respectively[17,21].

While an electrolysis cell uses an external electric power source to provide enough voltage to drive water splitting reactions; PECs and PPCs are able to perform water splitting with the overpotential provided by the light-excitation of charge carriers in the light-absorber[1]. The current highest solar-to-hydrogen (STH) efficiency of PEC is 18.3%[24].

1.3.2 Microscopic electrodes: particulate photocatalysts

The idea of PPC systems was first materialized by Lehn et al[25], Sato & White[26], and Domen et al[27] who demonstrated that water splitting by photo-excited electrons and holes is feasible as well by semiconductor particles (later known as photocatalysts[1] or light-absorbers[28]). Since few PPC systems can execute overall water splitting (OWS) by a semiconductor alone, loading one[25,29] or more cocatalysts[1,22] onto the light-absorber has been proved to be a highly effective approach to accelerate water splitting kinetics[22,30].

The occurrence of photocatalytic reactions on PPCs generally follows a pathway as illustrated in figure 1.5 b and via three steps[1]: (1) light absorption and exciton generation by photons with energy greater than the bandgap energy (E_g) of the light-absorber; (2) charge separation from exciton and migration to respective electron or hole traps on the light-absorber; (3) Surface redox reactions at redox sites located on the surface on the light absorber or the cocatalyst. To some extent, a cocatalyst-loaded light-absorber can be treated as a miniature version of a PEC system[22]. Nevertheless, several unique features of this system could potentially result differentiated kinetic and thermodynamic phenomena compared with those of the PEC systems.

In the following sections, we will present a full research work focusing on the cocatalyst-loaded GaNZnO PPC system for water splitting.

1.3.3 The economic advantage of particulate photocatalysts

Although PECs possess relatively high efficiency[24] and ease of gaseous products separation because of the nature of the separate electrodes[19], PPC systems still attract

tremendous efforts of research and development as such systems have an edge of economic competitiveness over other photocatalytic water splitting systems.

According to a comprehensive technoeconomic analysis done by Jaramillo et al, at the same energy conversion efficiency the combined cost (including capital, decommissioning, fixed operation, maintenance, and other variable costs) of hydrogen production via PPCs is only 40% of that of PECs equipped with solar concentrators[23]. At 10% or higher solar-to-hydrogen conversion efficiency, PPCs could generate hydrogen at less than 1.6 dollars per kg, and therefore make the produced hydrogen competitive with petroleum-based fuels[23].

Chapter 2: A View on Principles and Theories

2.1 The miniaturized electrolytic cell analogy

As discussed in Chapter 1, the loaded cocatalysts on the surface of the light-absorber play a role of electrodes where electrons or holes can be collected and used to drive redox reactions[1,14,22]. In this work, such locations where surface redox reactions happen are also referred as reduction site (cathode) or oxidation site (anode) towards which electrons or holes migrate (figure 1.5 b).

For decades[17,21,32], photocatalysts have been studied via an electrolytic cell analogy for the ease of obtaining quantitative data[31] and probing mechanism[32]. In this analogy, cocatalyst and light absorber are regarded as electrodes of an electrolytic cell counterpart where semiconductor a light-absorber and a cocatalyst (a metal or metal oxide) serve as electrodes. In addition, the light-absorber itself can provide necessary electromotive force upon irradiation. One classic example is: an n-type light-absorber serves as an anode performing oxidation reaction, while a cocatalyst (a metal or metal oxide) loaded on the light-absorber serves as a cathode performing reduction reaction[22]. With this concept, macroscopic PEC cells were constructed by connecting two electrodes (coated with a layer of semiconductor and a layer of cocatalyst respectively) together via external circuits[17,21,33]. A light source illuminates the light-absorber side, such that energetic excitons can be generated when the incident photon energy is greater than the bandgap energy of the light-absorber[1]. The energy difference between the valence band maximum and conduction band minimum dictates the energy/voltage that can be applied for driving photocatalytic reactions[23].

Half-cell reactions (i.e. hydrogen and oxygen evolutions) and/or overall water splitting are generally studied in aqueous solution with or without sacrificial reagents[1,]. In consistency with electrolytic water splitting[19,34], it is considered that a lower pH is beneficial for hydrogen evolution (i.e. proton reduction), while an alkaline condition facilitates oxygen evolution (i.e. hydroxyl oxidation).

2.2 Limitations of the electrolytic cell analogy

It is well-known that the (photo)electrolytic cell set-up offers indispensable advantages[17,21,32], including: the convenience of quantifying reaction kinetics by measuring the electrode current density, and the macroscopic demonstration of charge transfer phenomenon by observing on which electrode the hydrogen/oxygen is evolved[19]. However, for analyzing heterogeneous photocatalytic water splitting of PPC systems; critical limitations of this set-up may have also overshadowed important insights of water splitting by particulate photocatalyst systems. Hereby such limitations are summarized in the following sub-sections.

2.2.1 The Overlooked Heterojunction Formation

The first limitation is the overlooked interaction between cocatalyst and light-absorber. Usually, when a photoelectrolytic cell is constructed, the cocatalyst and/or the light-absorber are backed by a resin-supported metal alloy[35] (e.g., Au/Cr[36] alloy or In/Ag alloy[21]) in order to form an ohmic contact before connecting to an external circuit. Therefore, the interaction between the cocatalyst and the light-absorber is minimized, and the contact is expected to be ohmic[35]. Since the nature of an ohmic contact determines

16

that the electrons generated by and excited to the conduction band of an n-type semiconductor will fall onto the cocatalyst without being hindered by an energy barrier (e.g., Schottky barrier)[37]; the surface of the light-absorber then becomes a hole trap, whereas the surface of metal becomes an electron trap. This phenomenon has been confirmed in numerous photoelectrolytic cell experiments since 1972, taking Fujishima & Honda's first demonstration of water splitting via Pt/TiO$_2$ cell[21] as an example.

2.2.2 A Revisable Reaction Mechanism

The second limitation could be regarded as a biased view on water splitting mechanism extended from the first limitation. Based on the conclusion, reached by the photoelectrolytic cell systems, in which electrons always migrate from the light-absorber to the cocatalyst; well-accepted pictures elucidating the mainstream photocatalytic reaction mechanisms for cocatalyst/n-type semiconductor have been depicted by a similar schematic diagram over the years.

Figure 2.1 A generic example of charge transfer and half reactions happening on photocatalyst surface
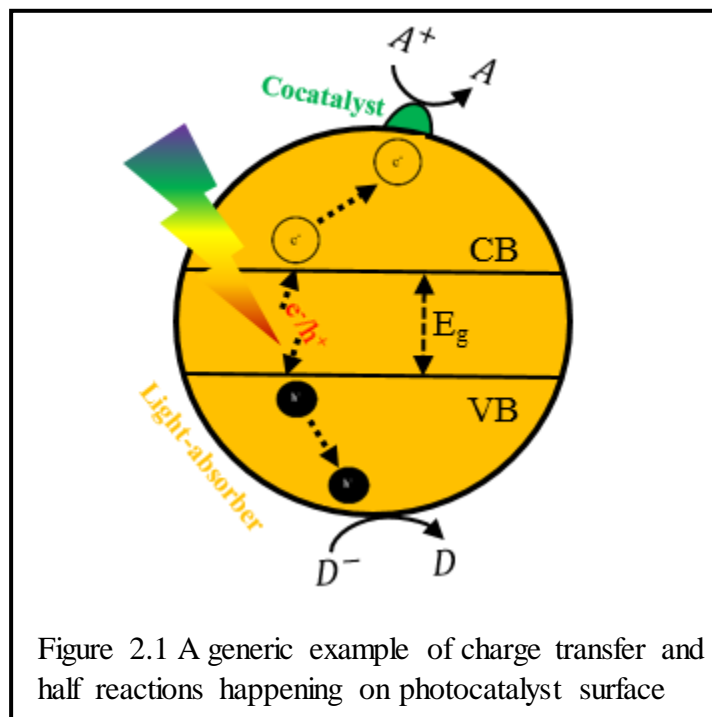
Under this model (figure 2.1), the loading of a cocatalyst creates electron-trapping sites that are able to perform hydrogen evolution reaction (i.e., proton reduction). The light-absorber becomes a site for oxygen evolution reaction (i.e., water oxidation), as photo-excited holes presumably remain on the light-absorber surface. Seemingly, the electrolytic cell analogy led to an electron transfer mechanism which advocates that electrons always migrate to the cocatalyst, making the cocatalyst a proton reduction site; while photo-generated holes remain on the light-absorber particle, filling the surface hole traps and initiating the oxidation reaction[22,38].

Although it is convenient to identify counterparts from both systems, particulate photocatalyst system (i.e. cocatalyst/light-absorber composite) is not simply a scale-down version of the photoelectrolytic cell. Importantly, the formation of cocatalyst|light-

absorber heterojunction[39,40] will induce phase mixing between cocatalyst and light-absorber, regardless of loading method (impregnation, photodeposition, or physical mixing). Therefore, it is expected that the direct contact of the nanometer-sized cocatalyst with light-absorber will cause probable electronic property modification at the interface, compared with the distant connection between anode and cathode in an electrolytic cell. In addition to the close contact between two materials, the particulate photocatalytic systems may also possess unique properties that deviate from their macro-scaled counterparts (i.e. photoelectrolytic cells), such as: intrinsic electronic structure, light absorption, optical scattering, and etc.

In a brief summary: even though PPCs have been usually treated as the down-sized PECs in literature[1,22] for the convenience of electrochemical analysis[22,32], the subtle while critical differences between the two systems exist and could lead to unusual kinetic phenomena overserved in this work.

2.3 A Solid Physics View: Energy Levels Re-alignment and Band-bending Theory

When two non-identical materials (e.g. conductors and semiconductors) come into contact, interfacial electron transfer occurs due to the Fermi level difference between the two materials[41]. Without external bias or light irradiation, the contact quickly reaches equilibrium and results in an aligned Fermi level for both materials. A space charge region (depletion or accumulation layer) simultaneously forms at the interface, causing

the nearby band edges to shift upwards or downwards. The resultant band profile appears

to be bent, which is referred as band bending in solid state physics[37,41].

Figure 2.2 Illustration of the principle of band-bending at material interface resulted from electron transfer: (a) before contact, (b) upon contact (non-equilibrium), (c) at equilibrium after contact (graph adapted from reference 37).

This phenomenon is schematically illustrated in figure 2.2 in which the contact

between an n-type semiconductor and metal is used as an example. If the Fermi level of a

semiconductor is lower than that of the metal (e.g., p-type semiconductor), the non-

equilibrium electron transfer will be reversed, causing the bands to bend down near the

interface[37,41]. If the contacting materials have identical Fermi levels, no electron transfer

will occur at interface, resulting no band-bending[37].

The band-bending schemes lead to two types of contacts—Schottky barrier and ohmic contact, schematically summarized in Figure 2.3:

Figure 2.3 Illustration of contact types as a result of band-bending: (a) Schottky barrier; (b) and (c) are ohmic contacts (graph adapted from reference 37 and 41). The red dotted arrows represent the assumed most probable electron transfer paths when the system is illuminated.
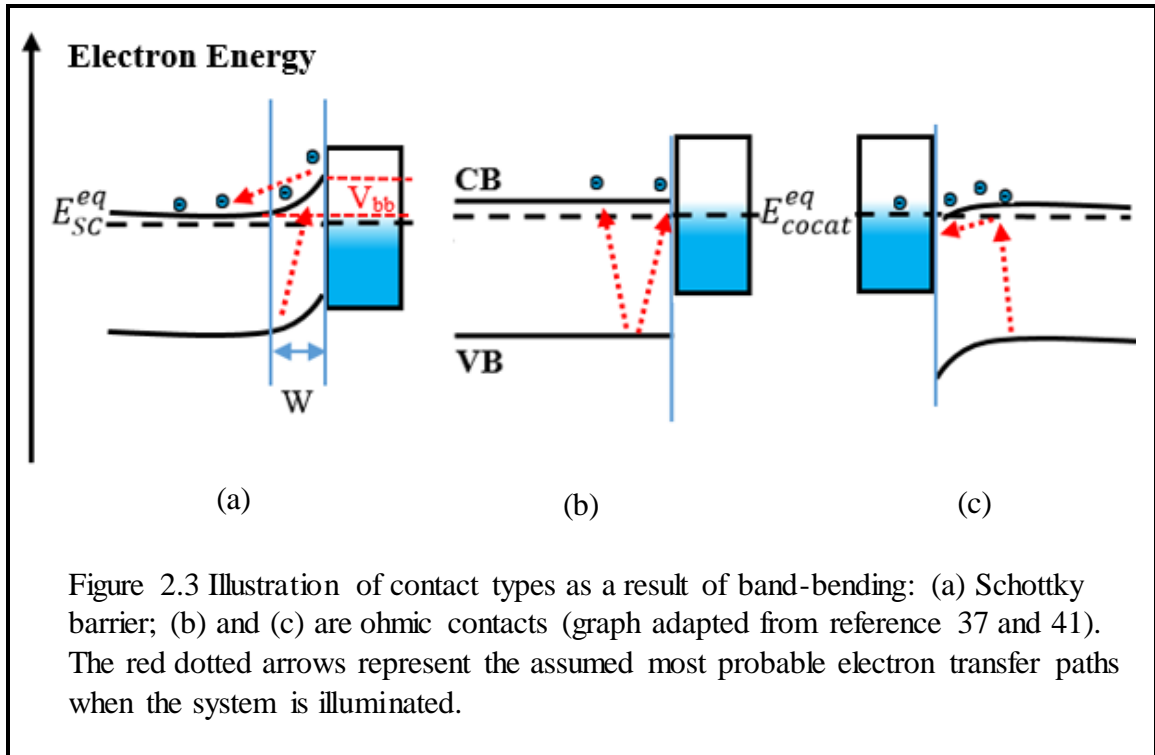
For our focused cocatalyst|GaNZnO junctions, we expect a bend-up band structure at the junction interface (figure 2.3 a) for most of the cases. As an n-type semiconductor[42], the Fermi level of GaNZnO is expected to located very close to the conduction band edge, and therefore is supposed to be higher than those of the cocatalysts (metals or metal oxides).

Although this work largely focused on the solid junctions formed between cocatalyst and GaNZnO; it is still worth to mention that the band-bending phenomena can occur at solution|photocatalyst interfaces. Such cases are summarized in figure 2.4:

Figure 2.4 Solution/adsorbate-induced band-bending schemes: an n-type semiconductor in oxidative (left) versus reductive (right) environments. (Graph adapted from reference 41)
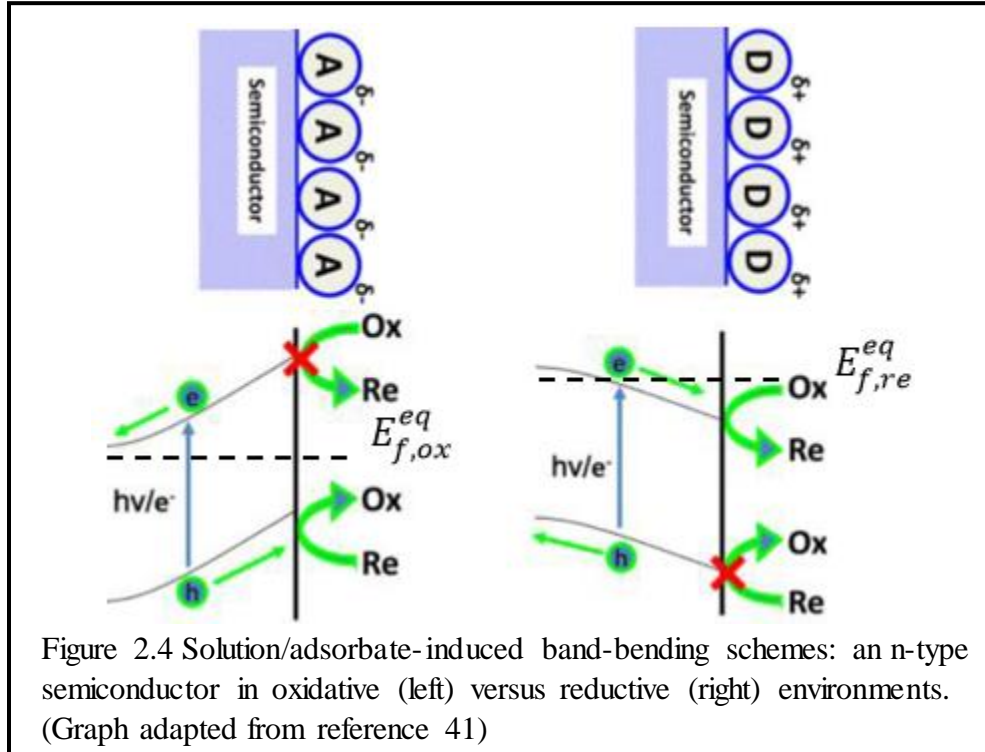
Theoretically the adsorbed electron acceptors (e.g., oxidizers) favor the oxidation half reaction on photocatalyst (i.e., light-absorber); while the electron donors (e.g., oxidizers) facilitate the reduction half reaction on photocatalyst at adsorbate|photocatalyst interface.

Chapter 3: Methodology and experimental approaches

3.1 Summary of Experiments

This chapter provides information of the light-absorber (GaNZnO), the cocatalysts, the synthesis of light-absorber and cocatalysts, characterization techniques, and the development of photocatalytic and photo-labeling experiments.

3.2 Selection of Light-absorber and Cocatalysts

3.2.1 Light-absorber

We revisited the water splitting mechanism of particulate photocatalytic system via the classic cocatalyst|light-absorber configuration where gallium zinc oxynitride (abbr. GaNZnO) is selected as a model light-absorber.

Gallium zinc oxynitride (GaNZnO), regarded a solid solution of gallium nitride (GaN) and zinc oxide (ZnO), was first developed by Doman et al in 2005[44]. GaNZnO was selected as a model light absorber owning to its featured physical and chemical properties, such as: a relatively small band-gap for visible light absorption[45], thermodynamically suitable band-edge positions[46] to perform overall water splitting reaction, and thermal stability (up to 700 degree Celsius)[47].

The abovementioned properties also ensure that the thermal treatment of GaNZnO at the calcination or hydrogen reduction stage for cocatalyst loading onto GaNZnO will not affect the intrinsic reactivity of the light-absorber by significantly modifying the crystal structure[47].

3.2.2 Metal and Metal Oxides as Cocatalysts

Metals and their respective oxides that had been previously studied in the literature of water electrolysis[48] were selected as cocatalysts loaded to GaNZnO,

including: platinum (Pt), rhodium (Rh), chromium (Cr), nickel (Ni), ruthenium (Ru), as well as their oxides. The electrolytic HER activities of the selected cocatalysts also varies: Pt has the highest exchange current density, whereas Cr is a presentative of the most inactive metals for HER[48].

Since this work focuses mainly on the mono-cocatalyst cases, one GaNZnO sample is loaded with only one cocatalyst for the later kinetic studies (except for Rh-Cr mixed oxide as a reference).

3.3 Material Synthesis

3.3.1 Light absorber (GaNZnO) synthesis

The synthesis of GaNZnO follows a modified method that was initially developed by Domen et al[49]. In brief, Gallium oxide (Ga_2O_3, Sigma Aldrich, purity 99.99%) and zinc oxide (ZnO, Sigma Aldrich, purity 99%) were pre-calcined at 550 and 600 degree Celsius respectively for 1 hour in air. The calcined metal oxides were then physically mixed together at 1:1 Zn:Ga molar ratio in a mortar. The oxide mixture (2 g) was then nitridated at an ammonia (NH_3) flowrate of 273 cubic centimeters (ccm) in a tube furnace at 850 degree Celsius for 15 hours. The post-nitridation power (GaNZnO) appears to be yellow, and is characterized by UV-Vis spectroscopy and XRD. The material synthesis procedures for GaNZnO and the cocatalyst-loaded GaNZnO are illustrated in Figure 3.1 on next page.
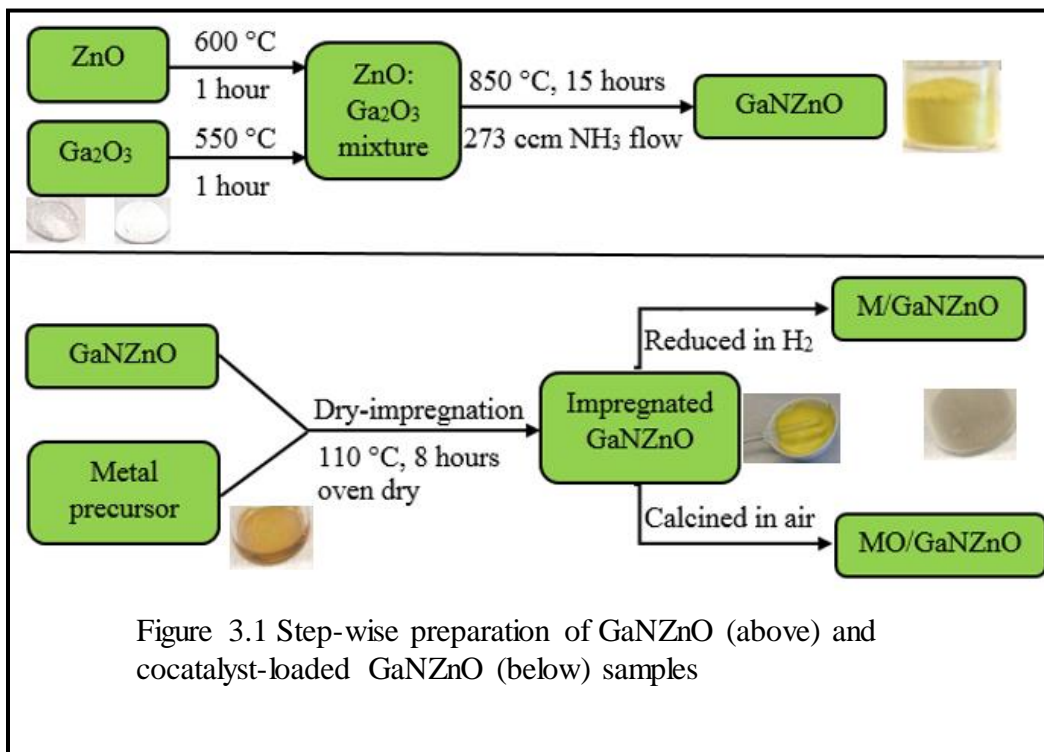
Figure 3.1 Step-wise preparation of GaNZnO (above) and cocatalyst-loaded GaNZnO (below) samples

3.3.2 Cocatalyst loading procedures

The loading of a cocatalyst was accomplished via a simple impregnation method used in a previous work[50] on photocatalytic watersplitting study. In order to minimize the negative effect on activity caused by ions (such as K^+, Na^-, and Cl^-), only metal nitrate salts were used to prepare the precursor solutions (figure 3.1) by dissolving adequate amount of metal nitrate salts into distilled water solvent.

Next, for every 100 mg of GaNZnO, 220 μL of the metal precursor solution was added. The precursor solution contains adequate amount of metal nitrate salt, such that the final metal loading was 1% wt. in most cases for metal-loaded GaNZnO sample (M|GaNZnO). During the impregnation process, a glass rod was used to vigorously stir the paste to ensure homogenous adsorption of metal precursor on GaNZnO particles. The

impregnated GaNZnO was oven-dried at 110 degree Celsius for 8 hours under vacuum; and was then ground by a pestle prior to the thermo-treatment processes.

To obtain the M|GaNZnO, the impregnated powder was reduced by hydrogen (H_2, flowrate at 100 ccm) at 300 degree Celsius for 2 hours. Whereas, for metal-oxide loaded samples (MO_x|GaNZnO), the impregnated samples were calcined in air at different annealing conditions summarized in table 3.1.

Table 3.1 Summary of metal oxide preparation conditions

Desired MO (Formula)	Annealing T (°C)	Time (hours)	Reference (#)
CrO_x	450	6	This work
NiO_x	400	3	50
$RhCrO_x$	350	1	30
RhO_x	350	1	30
RuO_x	400	6	50

The impregnation procedures and the calcination conditions together ensure the formation of mixed metal oxides (MO_x) on GaNZnO, and avoid resulting in the core-shell structure (e.g. rhodium as core and chromium oxide encircle the rhodium as shell) in this work.

3.3.3 Photo-labeling experiments

The purpose of photo-labeling experiments[51] is to track the migration phenomena of photo-excited charge carriers on the photocatalyst surface by photodepositing Pt from Pt^{4+} precursor—chloroplatinic acid (H_2PtCl_6, Sigma Aldrich, purity 99.9%). This process is also referred as photodeposition (PD) in this work. Such experiments were conducted

in a way that is very similar to the water splitting kinetics experiments. The protocol is described in the following paragraph.

For the photo-labeling experiment (2.5% Pt target loading as example), 5 μL of H_2PtCl_6 solution (8% wt.) was pipetted to 8 mg of photocatalyst (1% RhO_x|GaNZnO or GaNZnO) suspended in 60 mL distilled water. The mixture was vortexed for 1 minute and stirred for 30 minutes so as to ensure the adsorption of H_2PtCl_6 on the photocatalyst surface. The suspension was degassed in an air-tight photo-reactor back-filled with Argon (Ar, Air Gas, purity 99.999%), and was then illuminated by a metal halide lamp (MH100A, Dolan-Jenner, bulb power 150 W) for 24 hours to ensure that the Pt precursor is successfully reduced on the surface of the photocatalyst. The post-deposition suspension was washed and centrifuged for 4 times before loading to the TEM grid for STEM and EDS characterization detailed in section 3.4. The target loading, which is also the maximum theoretical loading of Pt, can be varied by adjusting the volume of Pt precursor solution. Several target Pt loadings (0.5%, 2.5% and 5%) were examined in order to optimize the PD results shown on the STEM and EDS images.

Figure 3.2 Schematic depiction of the photo-labeling experiment:
(a) RhO_x/GaNZnO before photodeposition with the presence of
the precursor; (b) and (c) RhO_x/GaNZnO after photodeposition
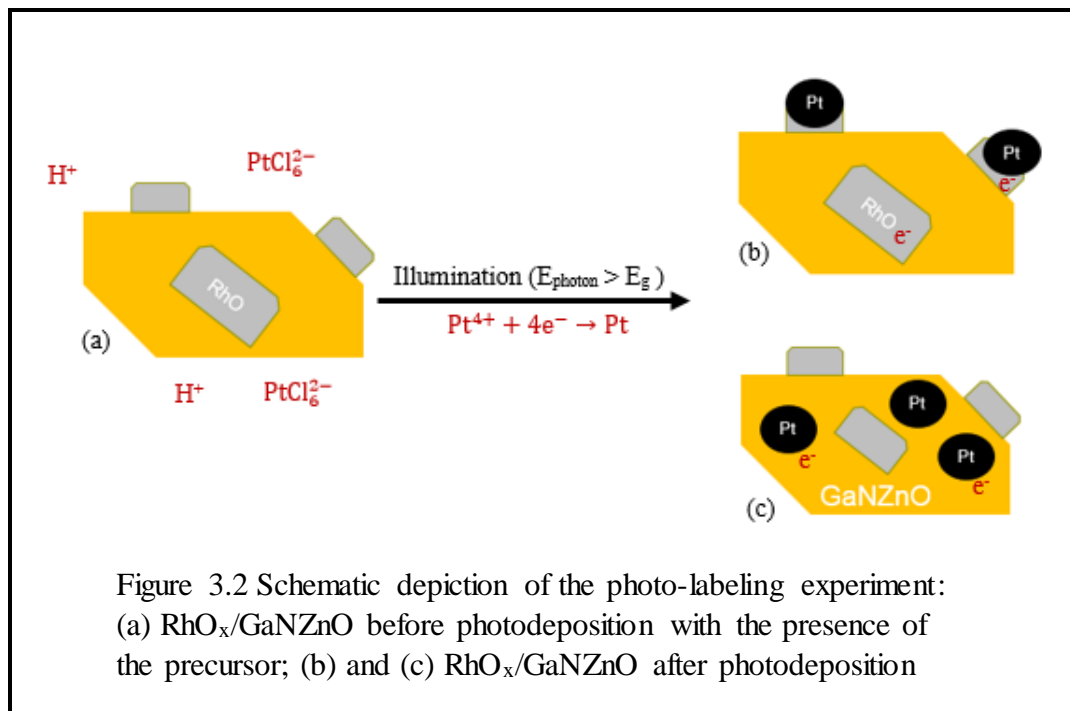
As depicted in Figure 3.2, the principle of these experiments states that the Pt^{4+}
species is reduced by conduction band electrons generated by the light-absorber. Thus,
the location of the Pt after the photodeposition (PD) process can provide direct evidence
of the electron transfer direction: either from the light-absorber to the cocatalyst (resulted
in Pt-RhO_x|GaNZnO structure), or stay on the surface of the light-absorber[51] (resulted in
RhO_x|GaNZnO-Pt structure).

3.4 Characterization Techniques

Various characterization techniques were applied to yield photo and physical properties of the samples, or to confirm the proposed charge transfer direction from the photo-labeling experiments.

3.4.1 Nitrogen physical adsorption

The GaNZnO sample underwent 4 hours of degassing at 300 degree C prior to the surface area measurement. The nitrogen physio-sorption onto the light-absorber (GaNZnO) was performed with Micromeritics ASAP 2020 under proper vacuum at 77 °K. By dosing nitrogen onto the sample step by step, the changes in relative pressure (P/P$_0$) was recorded, and fit to BET isotherm. The total surface area of GaNZnO was then calculated from the isotherm.

3.4.2 UV-Vis Diffuse Reflectance Spectroscopy (UV-VIS DRS)

The UV-VIS DRS was applied to analyze the photo-optical properties of the light-absorber. The sample was scanned for a spectra ranging from 300 nm to 700 nm with a Thermo Scientific 300 spectrophotometer equipped with a Harrick Praying Mantis^{TM} chamber. The collected absorption and reflectance spectra can be processed by Kubelka-Munk (K-M) theory, which yields the band-gap energy (E$_g$) of the light-absorber[52].

3.4.3 X-ray Diffraction (XRD)

The crystallinity of GaNZnO was checked by XRD technique (Cu X-ray source, wavelength = 0.14 nm). For the GaNZnO sample in the present work, 45 kV high tension and 30 mA current emission were the parameters set for X-ray scan from 10 to 70° angle

(2θ) at 0.0275 second per step. The peak intensities over 2θ angle compose the XRD spectra of the sample.

3.4.4 Transmission Electron Microscopy (TEM)

In order to obtain a visualization of the morphology and size of the photocatalyst particles, TEM technique was employed for GaNZnO as well as the loaded GaNZnO samples. All bright-field TEM images presented in this work were taken at Central Facility for Advanced Microscopy and Microanalysis (CFAMM) with FEI Tecnai 12 TEM (120 kV acceleration voltage).

3.4.5 Scanning Transmission Electron Microscopy (STEM)

The morphology and dark-field images of the samples from the photo-labeling experiments were obtained by STEM equipped with a High Angle Annular Dark Field (HAADF) detector. The surface element composition and mapping were analyzed with Energy-dispersive X-ray Spectroscopy (EDS) which was enabled by the X-ray Spectrometer system attached to the STEM. In this work, the 0.5% and 2.5% Pt PD samples were characterized via FEI Titan Themis 300 at CFAMM; while the 5% target loading samples were imaged via JEOL 2100F at CEMMA, USC.

3.5 Photocatalytic Reactivity Experiments

Photocatalytic reactivity experiments are designed for the investigation of water splitting kinetics of PPC systems. The main observables, including the headspace gas species concentrations, illumination times, headspace pressures, and temperatures, can provide useful kinetic performance of each sample. Three categories of such experiments were executed, namely: overall water splitting (OWS), hydrogen evolution (HER), and oxygen evolution (HER) reactions. More details of the experimental set-ups are documented in the following sections.

3.5.1 Design of photocatalytic reactor and light-source specifications

All photocatalytic reactions and photodeposition (PD) experiments were performed inside a semi-batch reactor (figure 3.3 a) specifically designed for this project. The reactor material is borosilicate glass which can transmit light with wavelength greater than 284 nm, which was checked by UV-Vis transmission measurement. The reactor is equipped with a pressure gauge for real-time headspace pressure monitoring, and a sampling port from which gas samples could be taken and transferred by a gas tight syringe. The capacity of the reactor is 121 mL.

During the photocatalytic experiments (OWS, HER, and OER), this reactor was side-illuminated by a metal halide lamp (MH100A, Dolan-Jenner, bulb power 150 W). A custom-built light guide (1 inch in length) is used to channel the light from the lamp outlet to the reactor wall. The intensity of illumination at the reactor wall was measured to be 700 mW or 640 mW/cm^2. Since the lamp is not equipped with any optic filter, a full output spectrum (figure 3.3 b) was utilized for all photocatalytic reaction.
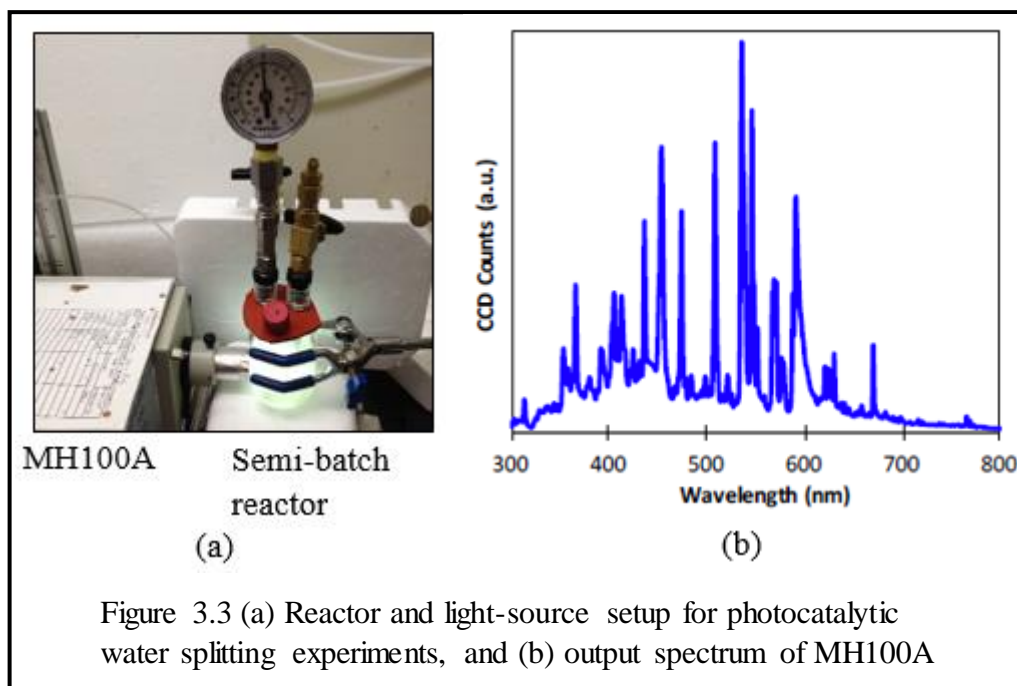
Figure 3.3 (a) Reactor and light-source setup for photocatalytic water splitting experiments, and (b) output spectrum of MH100A

3.5.2 Reactor background, gas sampling and analysis

Prior to the execution of every water splitting experiment (OWS, HER, or OER), the reactor (with photocatalyst suspension inside) is degassed under -29 inch Hg vacuum for 10 minutes and through a 7-cycle vacuum and Ar (or He) back-fill process to minimize the presence of air species. Yet a mild increase of the background oxygen and nitrogen concentrations in the reactor headspace over time was always observed. Since

the background N_2:O_2 ratio remains constant over time, we decided to obtain the net

oxygen concentration (oxygen evolved from water splitting) in the head space by

subtracting the simulated oxygen concentration (based on the constant N_2:O_2 ratio) from

the total oxygen concentration in the headspace by applying equation 3.1:

$$net\ O_2\ (ppm) = total\ O_2 - \frac{background\ N_2}{background\ N_2:O_2}$$
<div align="right">Eq. 3.1</div>

A sample plot is provided in figure 3.4 (on next page), demonstrating the effect of

Eq. 1.9 for calculating photocatalytic oxygen evolution for OWS experiments. The

dashed lines represent the background gas evolutions. The background oxygen (green

dashed line) net oxygen evolution is subtracted from the total oxygen (blue solid line) in

order to correct the real oxygen evolution (purple line) from photocatalytic WS. After

converting the concentration unit to µmol/g-min by applying the ideal-gas law, the slope

of the gas evolution is generally regarded as the steady-state WS gas generation rate.

Figure 3.4 A typical gas accumulation plot in reactor headspace showing how the net oxygen evolution (purple line) is calculated.
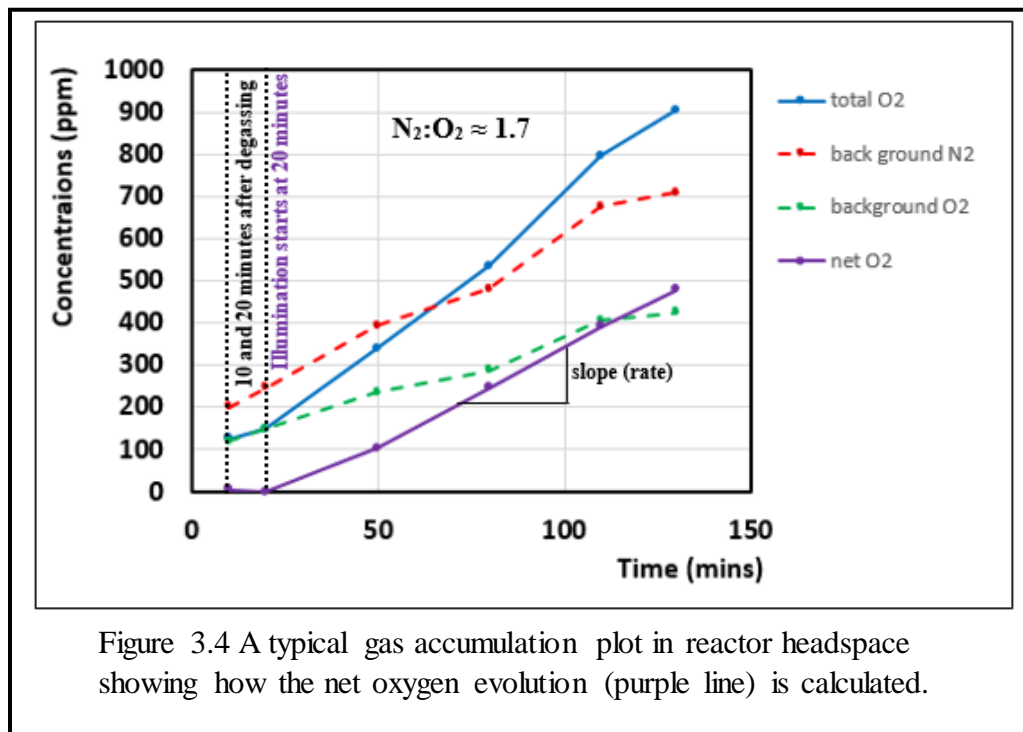
The hydrogen evolution rate is calculated from a similar approach without the background subtraction step, since there is no background hydrogen species.

Gas concentration in the reactor headspace is monitored through an off-line GC (MG 8610 C, manufactured by SRIGC) with HID and TCD detectors (carrier gas: He) or with one TCD detector (carrier gas: Ar), and two MX-13 columns in series. An air-tight syringe (VICI Pressure-Lok® Precision Analytical Syringe) was used to transfer the gas sample from the reactor to the GC injection port.

3.5.3 Overall water splitting experiments (OWS)

The OWS process refers to the direct cleavage of water molecules by photocatalyst systems without any sacrificial reagent, in which water is both oxidized and reduced into oxygen and hydrogen[1]. The OWS proceeds through Eq. 1.5 to Eq. 1.7.

Prior to photocatalytic reactions, the catalyst suspension (10 mg powder in 60 mL distilled water) was sonicated for 10 minutes to ensure a homogeneous condition. The reactor (with the suspension inside) was then degassed through dose-vacuum cycles (He or Ar as dosing gas) detailed in section 3.5.2. After degassing, the headspace pressure of the photo-reactor was re-adjusted to 11 psi with inert gas (He or Ar). The suspension was stirred by two Teflon-coated stir bars at 1200 rpm during the equilibration period (20 minutes) as well as the illumination period. For all water splitting experiments, no mechanocatalytic effect[53] was observed prior to illumination (i.e., during the equilibration period under dark condition). Therefore, gas evolutions from the suspension are resulted from the photocatalytic water splitting phenomenon.

3.5.4 Half-reaction experiments (HER and OER)

The water splitting half-reactions refer to the hydrogen evolution reaction (HER) and oxygen evolution reaction (OER). The former case uses a sacrificial reagent (SR) which scavenges the photogenerated holes from the photocatalyst, so that the photogenerated electrons are remained for the reduction of water, i.e. hydrogen evolution; the latter case uses an electron scavenger to facilitate the oxidation of water by photogenerated holes[1]. The sacrificial reagents are also referred as hole and electron scavengers in this work.

For this study, compounds used as SRs for half reaction experiments (HER and OER) are sodium sulfite (Na_2SO_3, Sigma-Aldrich, 98% minimum purity) and silver nitrate ($AgNO_3$, Lab Science, 99% minimum purity) respectively. The energetics of species (shown as redox couples) involved in OWS, HER, and OER are schematically illustrated in figure 3.5:

Figure 3.5 Band-edge positions of GaNZnO (left), redox potentials (right) of water (black bars), and redox couples that can be used as SRs. (Green bars: hole scavenger redox potentials; blue bar: electron scavenger redox potential)
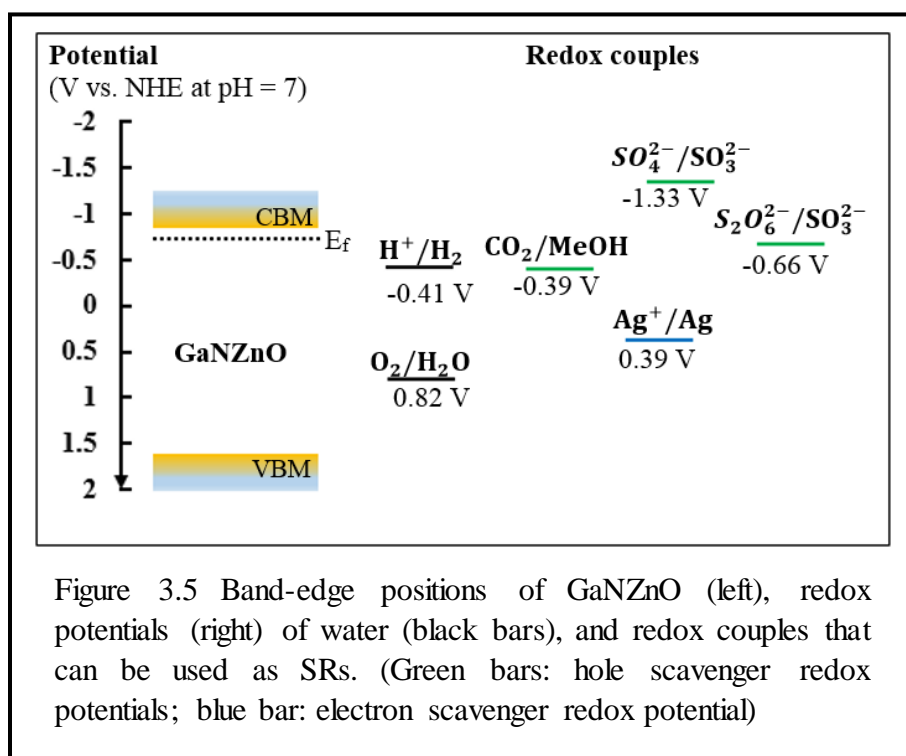
The band-edge positions[54] of GaNZnO are represented by conduction band minimum (CBM) and valence band maximum (VBM), assuming the Fermi level of GaNZnO is approximately 0.1 eV below CBM and does not vary significantly with pH as other metal oxides behave in aqueous solution[57]. The numerical values of redox

potentials[42,55,56] for SRs are re-calculated from the known literature by applying Nernst relation[57] which corrects for the pH effect.

Valuable thermodynamic information can be interpreted from Figure 3.5, as all energy levels are referenced to the normal hydrogen electrode (NHE). On an energy (potential) scale, the more negative potential at which a substance is located, the more thermodynamically feasible for that substance to be oxidized by photogenerated holes, vice versa[57].

3.5.4.1 HER experiments

In the reduction half reaction water splitting experiments, the HER is promoted while OER from water needs to be suppressed[1]. This fact requires SR species to be more oxidizable than water. From figure 3.5, it is noticeable that the oxidation potentials of methanol (MeOH) and sulfite (SO_3^{2-}) are both more negative than that of water, therefore both compounds are thermodynamically suitable to be hole scavengers.

In addition, an effective HER SR should be able to not only actively accept holes from the photocatalyst system, but is also preferably inorganic, as organic SRs can potentially release hydrogen from themselves through C-H bond breaking[58]. For instance, aqueous MeOH could be oxidized by photogenerated holes[59] through:

$$\text{MeOH} \xrightarrow{\ h\nu,\ h^+\ } \text{HCHO} + \text{H}_2 \qquad\qquad \text{E.q. 3.2}$$

The formaldehyde (HCHO) can be further decomposed to carbon dioxide and hydrogen[59], which transform the HER half reaction to methanol decomposition rather than water splitting. Therefore, in order to ensure that the water splitting reaction is

38

studied, it is crucial to use an inorganic SR that will not contribute to photocatalytic hydrogen evolution.

We studied the effectiveness of the six SRs that were previously reported in literature[42,56,58-62] to promote hydrogen evolution, namely MeOH, sodium iodide (NaI), sodium sulfite (Na_2SO_3), sodium metabisulfite ($Na_2S_2O_5$), sodium hypophosphite ($Na_2H_2PO_2$), and sodium bisulfite ($NaHSO_3$). The concentration of all inorganic SRs are 0.1 M. The methanol solution has a concentration of 10 % by volume. The results are summarized in figure 3.6.

Figure 3.6 Photocatalytic hydrogen evolution rates (HER) of 1%Rh1.5%CrO_x|GaNZnO sample in various sacrificial regent solutions. The HER of OWS by the same sample (marked as none) is served as a reference.
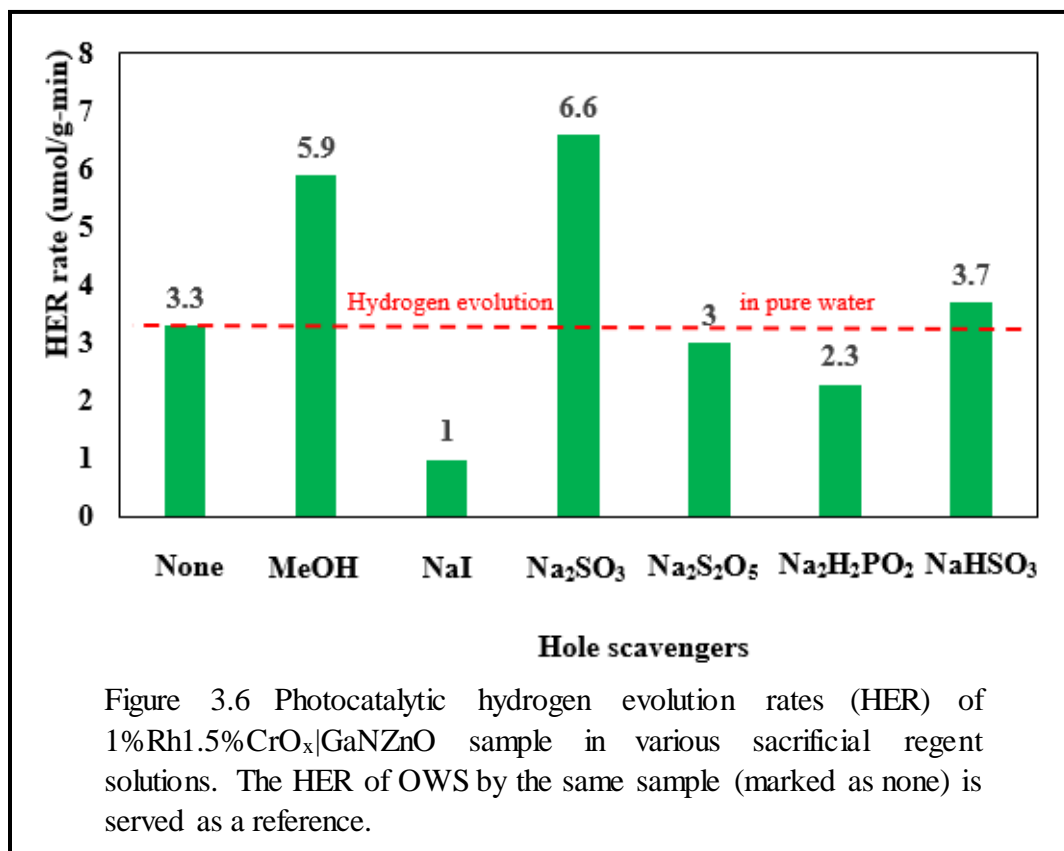
Among the inorganic SR candidates, only the presence of sodium sulfite and sodium bisulfite improved the rate of HER compared with the rate in OWS. Sulfite SR demonstrates significant HER kinetics (i.e., a 100% rate increase compared with OWS) for the half reaction. Thus, we selected sodium sulfite as SR for all HER experiments.

Nearly all HER experiments of this work, unless specifically mentioned, were conducted in 0.1 M Na_2SO_3 dissolved in distilled water. The Na_2SO_3 solution is always freshly prepared right before every experiment, such that the oxidation of sulfite by air is minimized. The as-prepared Na_2SO_3 solution has a pH of 9.5 measured by a pH meter. The protocol of HER experiments follows the same procedure developed for OWS experiments, which could be referred from the previous sections.

For buffered HER experiments, the Na_2SO_3 is dissolved in a phosphate buffer solution (0.1 M total phosphate concentration) which is prepared by adding adequate amounts of sodium dihydrogen phosphate monohydrate ($NaH_2PO_4 \cdot H_2O$, Spectrum, 98% minimum purity) and disodium phosphate (Na_2HPO_4, Spectrum, 99% minimum purity) into distilled water. The Na_2SO_3 containing buffer solution (0.1 M Na_2SO_3 and 0.1 M phosphate) has a measured pH of 7.3 prior to photocatalytic reaction.

3.5.4.2 OER experiments

In the oxidation half reaction experiments, oxygen evolution reaction (OER) is accelerated, while hydrogen evolution reaction (HER) from water is suppressed by using an electron scavenger[1]. As suggested by figure 3.5, silver nitrate ($AgNO_3$) is thermodynamically far more feasible to be reduced than water (0.39 V vs -0.41 V)[42,55,56], and therefore selected as electron scavenger for OER experiments in this work.

The protocol of OER experiments follows the same procedure developed for OWS and HER experiments, which could be referred from the previous sections. Solution of $AgNO_3$ has an initial concentration of 0.1 M. The duration of OER experiments is up to 50 minutes, which is shorter than that of OWS (2 to 4 hours) and HER (2 hours). The shorter illumination time is to avoid the excess Ag deposition on the photocatalyst, reducing the photocatalytic activity of the PPC systems[50].

All water splitting kinetic rates are averaged from triplet measurements, and are presented in Chapter 4. All gas evolution rates are reported with the unit of μmols of gas evolved per minute of illumination per gram of photocatalyst (μmol/min-g).

Chapter 4. Results and Discussion

The results from characterizations and water splitting reactions are documented in section 4.1 and 4.2 of this chapter. The latter is also discussed with existing theories, our hypotheses, approach (section 4.3) and proposed mechanism revision (section 4.4) to properly explain the observed kinetic results.

4.1 Characterization Results of GaNZnO

The synthesized GaNZnO power is first scanned via XRD technique in order to obtain the XRD spectrum (figure 4.1) of GaNZnO.

Figure 4.1 XRD spectra of GaNZnO samples nitridated for 5, 10 and 15 hours.
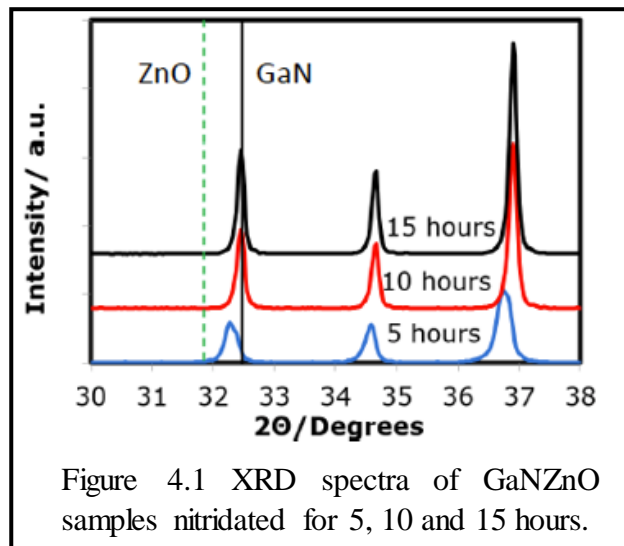
The characteristic peak in between the ZnO and GaN peak degrees confirms the crystallinity of the sample, and the formation of crystalline GaNZnO. Both the 10-hour and 15-hour nitridated samples exhibit similar XRD patterns and good crystallinity.

The photo-optical properties of GaNZnO are provided by applying UV-Vis spectroscopy. In consistency with the XRD results, the 10-hour and 15-hour nitridated samples possess very similar photon absorption abilities (figure 4.1 a). The collected reflectance data are used to generate Kubelka-Munk plot[52] against photon energy on the horizontal axis (figure 4.1 b), from which the band gap energy (E_g) of GaNZnO can be deduced.

Figure 4.2 (a) UV-Vis spectra of GaNZnO samples nitridated for 5, 10 and 15 hours; (b) K-M plot of GaNZnO sample (15-hour nitridation)
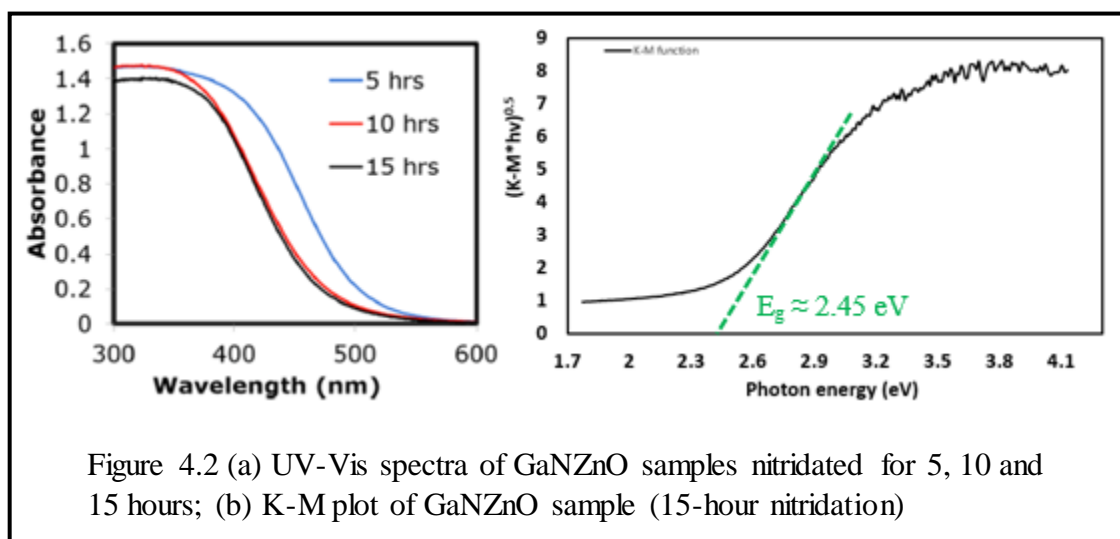
The band gap energy of the 15-hour nitridated sample is approximately 2.45 eV. This sample is also used in all kinetic experiments. According to BET surface area measurement, the synthesized GaNZnO has a total surface area of 6.3 m^2/g.

The TEM images of the sample are displayed in Figure 4.3 below, from which one can expect the average particle size of GaNZnO ranging from 20 nm to 100 nm.

Figure 4.3 The selected regions of TEM images for a GaNZnO sample. The scale bar in (a) is 50 nm, and 10 nm in (b).
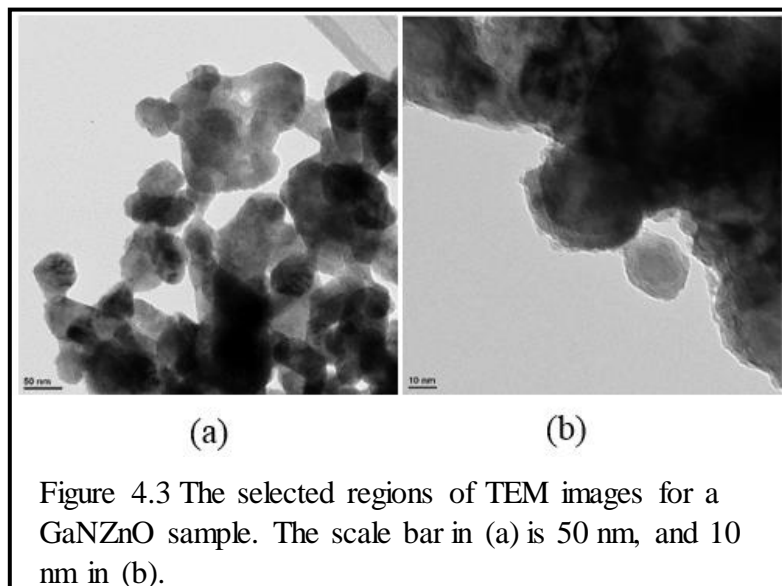
4.2 Water Splitting Kinetics and Discussions

The unusual kinetic phenomena observed from the overall watersplitting (OWS) and half-reaction (HER and OER) experiments contradict the outcomes that had been predicted by the electrolytic cell analogy as previously mentioned in Chapter 2. The processed kinetic data and photo-labelling experiment (PLE) results are presented and discussed in the following sections of Chapter 4.

4.2.1 The Surprising Results: Inactive Metallic Cocatalysts

As GaNZnO demonstrates no OWS activity without loading cocatalysts[44,49]; and water splitting kinetics of GaNZnO PPC systems was believed to be determined only by the reduction half reaction (i.e., HER) due to its n-type semiconductive nature[63]. We first

loaded GaNZnO with metallic cocatalysts which serve as cathodes, since if the macroscopic electrolytic cell analogy is totally correct, one can expect that photo-generated electrons will travel to the metal cocatalyst where proton reduction reaction occurs, and water splitting reaction on GaNZnO will no longer be limited by the reduction half reaction. The classical scheme may also assume the energy loss of the migrating electrons is minimized, since the Fermi levels of metals (referred as work functions)[48] are typically located much lower than that of n-type semiconductors (e.g. GaNZnO, TiO_2, ZnO, and etc.) on an energy scale and thus a thermodynamically favorable charge transfer process. Since GaNZnO has appropriate VB and CB positions for water reduction and oxidation, once the charges (i.e. photo-generated electrons and holes) are successfully separated by cocatalysts, water splitting proceeds through mechanisms demonstrated in figure 2.1 that is: photogenerated electrons will migrate to the cocatalyst where water reduction (i.e., HER) happens, while photogenerated holes remain on the surface of GaNZnO, oxidize water and release oxygen (i.e., OER)[63].

Yet, according to our conducted OWS experiments (unpublished data), all metallic cocatalysts loaded on GaNZnO failed to initiate detectable OWS activity under illumination. Furthermore, platinum (Pt), which is believed to be the most efficient hydrogen evolution catalyst in electrochemical water splitting[48], was unable to activate water cleavage. The inactivity of various metal cocatalysts when coupled with GaNZnO is a consistent observation with the previous results discussed by Domen et al in a previous study[30].

Such unusual phenomenon could not be explained properly with the existing electrolytic cell theory, we started to consider the following hypotheses for the cocatalyst-loaded n-type light absorber (cocatalyst|GaNZnO) systems: (1). Overall water splitting needs to be initiated by the oxidation half reaction rather than the proton reduction half reaction. (2). Even the light-absorber has n-type semiconductive photoelectrical properties, the reduction half reaction may not be the only rate-limiting step for water splitting. (3). If water splitting could be limited by the oxidation half reaction, then the reaction kinetics (represented by HER) are expected to be improved by introducing a more oxidizable reagent (i.e., SR) other than water. (4). Cocatalyst-semiconductor junction (e.g., cocatalyst|GaNZnO) formation at the interface of the cocatalyst and the light-absorber can potentially impact charge transfer direction and reaction kinetics.

In order to testify the validity of the above-mentioned hypotheses, we not only studied the kinetics of cocatalyst|GaNZnO PPC systems in OWS, HER, and OER conditions (section 4.2); but also explored the charge transfer phenomena impacted by the junction formation (section 4.3) via the photo-labelling experiments.

4.2.2 The Initiation of OWS Activity by Water Oxidation

We demonstrated that GaNZnO PPC systems remained inactive for photocatalytic water cleavage until certain metallic cocatalysts were oxidized thermally as detailed in the experimental section. Figure 4.4 presents the OWS activity achieved by the selected metal oxide cocatalysts below.

Figure 4.4 The achieved water splitting by metal-oxides loaded GaNZnO. All metal loadings are 1% by weight.
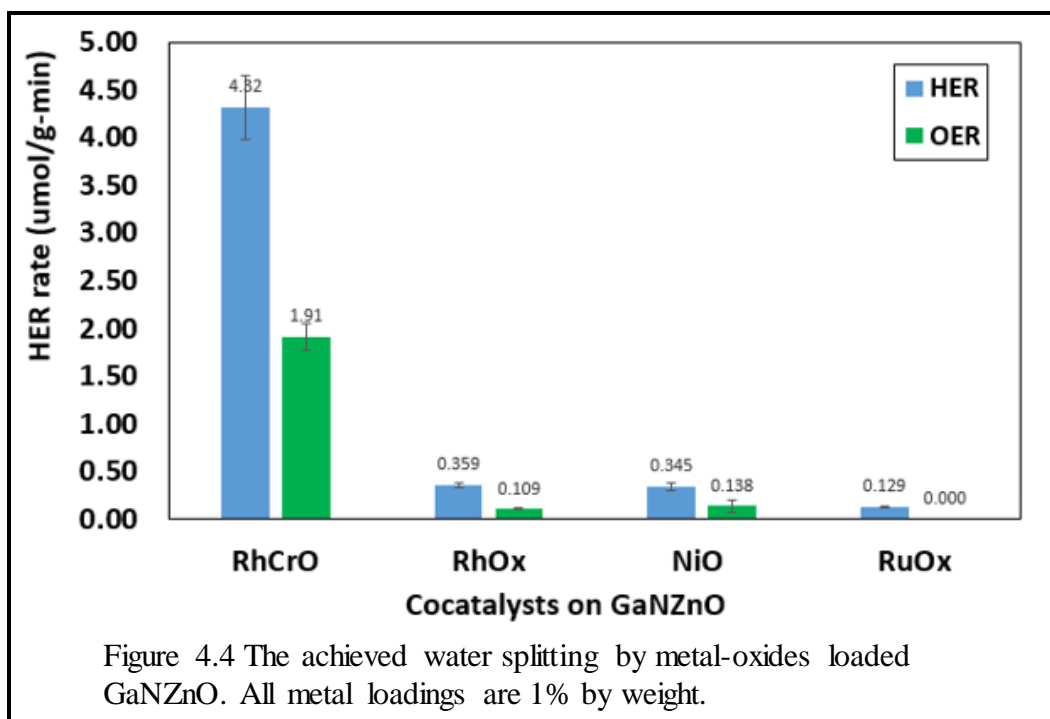
Our experiments demonstrated that NiO, RhO_x, RuO_x, and $RhCrO_x$ have hitherto shown detectable gas evolution activity in pure water. Except for the inert Cr_2O_3, metal oxides have been generally implemented as active oxygen evolution cocatalysts in both electrolytic[64] and photoelectrolytic water splitting processes[22]. From our photocatalytic experiments, it is evident that the water splitting process by cocatalyst|GaNZnO particulate systems is initiated by oxygen evolution reaction in which both O-H bonds

need to be broken before the formation of molecular hydrogen. Notably, such oxygen-evolving-first phenomenon is consistent with the water splitting reaction performed in PS II of plants, in which water is split into oxygen and protons[11]. Thus, the OWS reactions indicates the water splitting process is initiated by the oxidation half reaction (i.e., water oxidation).

4.2.3 The Greatly Improved Hydrogen Evolution Reactions (HER) by Lowering the Oxidation Half-reaction Barrier

To explore the hypothesis that the proceeding of water splitting reaction could be facilitated or initiated by the forerunning oxidation half reaction, we decided to design and execute multiple sets of HER experiments with the working metal-oxide cocatalyst|GaNZnO systems by introducing a SR species that is more thermodynamically oxidizable by water.

Sodium sulfite was chosen as sacrificial reagent (SR) for the HER experiments in this study. As mentioned in previous chapter 3, sodium sulfite not only has a more negative redox potential (figure 3.5), but also contains no C-H bonds which may attribute to the non-water splitting hydrogen evolution. Methanol and other organic SRs, on the other hand, could potentially become a hydrogen donor upon C-H bond cleavage.

During HER experiments, the water oxidation does not happen. Instead, oxidation half reaction proceeds through the following photo-anodic half reactions[61]:

$$SO_3^{2-} + 2OH^- \xrightarrow{2h^+} SO_4^{2-} + H_2O \qquad \text{Eq. 4.1}$$

$$2SO_3^{2-} \xrightarrow{2h^+} S_2O_6^{2-} \qquad \text{Eq. 4.2}$$
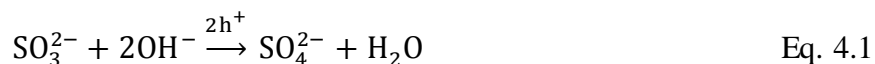
Sulfite oxidation results in the production of sulfate (43%) and dithionate (57%). Both products are assumed to be inert without participate in the reverse reactions. The reduction half reaction proceeds through Eq. 1.9, which yields hydrogen.

The HER kinetics of the working cocatalysts in different solution conditions (0.1 M sulfite, 0.1 M sulfite with 0.1 M phosphate buffer, and distilled water) are compile in Figure 4.5.

Figure 4.5 HER rates of cocatalysts loaded GaNZnO in different solution conditions (Blue: 0.1 M sulfite; Orange: 0.1 M sulfite and 0.1 M phosphate buffer; Green: water only). All metal loading is 1%.
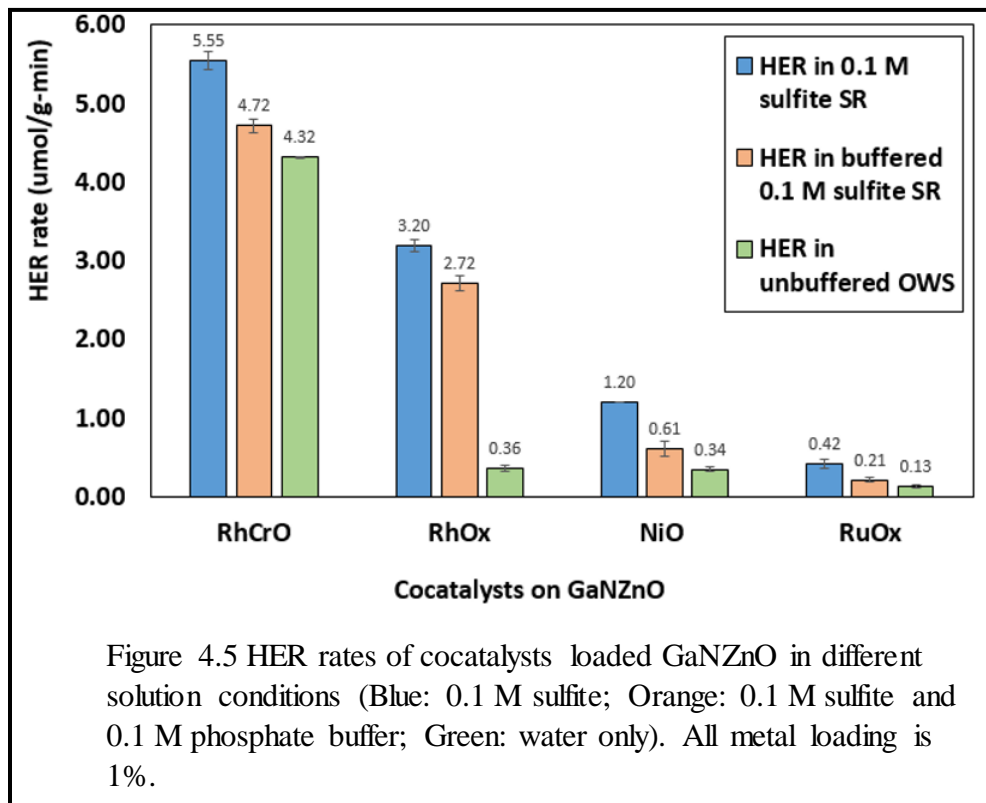
The HER results clearly demonstrates the kinetics sensitivity of the cocatalysts in HER environment. The HER rate ranking: $RhCrO_x > RhO_x > NiO_x > RuO_x$, is consistent with hydrogen evolving rate in OWS environment. It was also noticed that the HER improvements differentiate among the working cocatalysts. In 0.1 M sodium sulfite aqueous solution, $RhCrO_x$ binary oxide still outperforms any other mono cocatalysts. Nevertheless $RhCrO_x|GaNZnO$ system gained the least kinetic improvement; whereas the mono metal-oxide cocatalyst groups demonstrated rather significant reaction rate increases of over 200 percent, and at least 13-fold HER rate increase (RuO_x as an example) compared with the bare GaNZnO (0.04 μmol/min-g without any cocatalyst) when sulfite is present. In buffered condition, the HER rates suffered from the lowered effective sulfite concentration.

Figure 4.6 The influence of initial solution pH on HER rates of 1%Rh1.5%CrO_x loaded GaNZnO
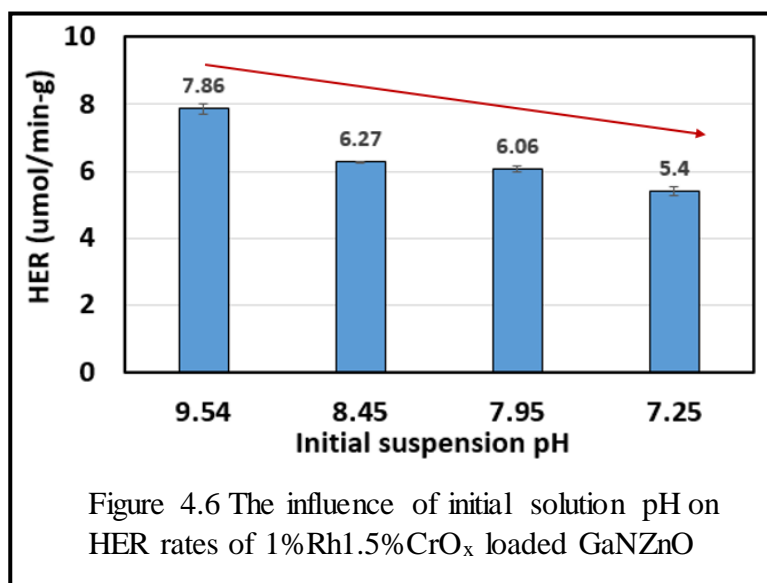
One set of pH dependent experiments was also conducted in order to study the pH dependence of HER. In all runs, the initial sulfite concentration was kept same at 0.1 M.

Kinetic data plotted in figure 4.6 reveals a moderate pH dependence of HER kinetics. It should be pinpointed: as pH decreased from 9.5 (no buffer) to 7.25 (with 0.1 M buffer), the actual sulfite concentration is approximately 25% lower than the nominal solution concentration[56]. Thus, the HER is more impacted by the effective concentration of sulfite rather than pH variation.

Judging from the variable HER rates of cocatalyst|GaNZnO PPCs, it is obvious that the hydrogen evolution kinetics are sensitive to the cocatalyst species in water as well as in SR solutions. By lowering the oxidation barrier of the reaction with sulfite oxidation, we demonstrate that the rate of water splitting can be improved greatly.

4.2.4 The Cocatalyst-insensitive Oxygen Evolution Reactions (OER)

The silver cations (Ag^+) in the solution can be readily be reduced via photo-cathodic reaction (Eq. 4.3), yielding oxygen (i.e., oxygen evolution) and metallic silver[65].

$$4Ag^+ + 4OH^- \xrightarrow{4e^-} O_2 + H_2O + 4Ag^0 \qquad\qquad \text{Eq. 4.3}$$
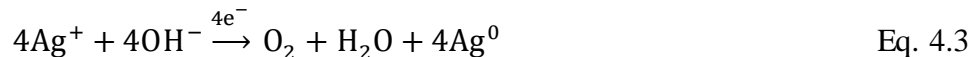
Since the reduction potential of Ag^+ is 0.8 V more positive than that of water (refer to figure 3.5), no water molecules or protons will be reduced. Therefore, no hydrogen will be produced during OER.

While HER is cocatalyst-sensitive for the working cocatalysts; experimental results in Figure 4.7 presented an overall insensitive phenomenon on OER kinetics with respect to cocatalysts in 0.1 M silver nitrate (AgNO$_3$) solution.

Figure 4.7 OER rates of cocatalysts loaded GaNZnO and bare GaNZnO (as reference) in 0.1 M nitrate solution. All metal loading is 1% for cocatalyst cases.
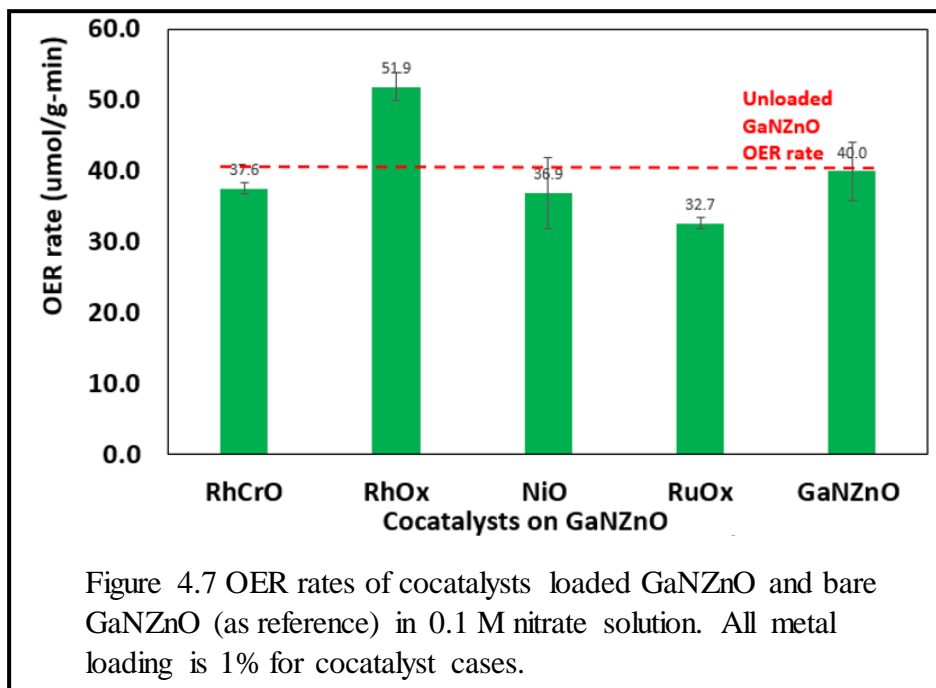
Except for RhO$_x$ which improved OER rate by 29.9%, other cocatalysts saw no improvement or negative impact on OER. Compared with the HER data, OER half reaction is relatively insensitive towards cocatalyst species. By introducing a more reducible sacrificial species, water splitting (indicated by OER) kinetics do not see significant improvement via cocatalyst loading.

The relatively insensitive OER with respect to cocatalyst species may suggest that the cocatalyst loading will not accelerate the silver reduction process (Eq. 4.3) as GaNZnO surface possibly provides sufficient electron trap sites for Ag$^+$ reduction.

4.2.5 The Possible Change in Charge Transfer Phenomena Induced by

Cocatalyst-Semiconductor Junction Formation

Demonstrated by the improved WS rates in both OWS and HER cases, the direct contact between metal oxides and light-absorber can create more effective heterojunctions for charge separation and photocatalytic reactions. As previously mentioned in Chapter 2, such micro-junctions could be p-n, n-n, Schottky, or Ohmic, depending on intrinsic material properties as well as the actual interface structure after synthesis. Since GaNZnO is an n-type semiconductor with a relatively high CB (compared with TiO_2, ZnO, $BiVO_4$, TaON, and many other n-type semiconductors)[1,54], it is reasonable to assume a high Fermi level (typically 0.1-0.2 eV below CB edge[66]) for an n-type semiconductor; whereas the Fermi levels of the working cocatalysts (metal or metal oxides) are believed to be lower than that of GaNZnO. According to theories of solid-state physics and relevant research works summarized by Yates et al, the upward band-bending (near the interface) at GaNZnO side is expected[41]. Thus, in certain cases, it is photo-generated holes that migrate to the cocatalyst side and perform oxidation reaction rather than proton reduction.

4.3 Revelation of Charge Transfer Direction via Photo-labelling Experiments

In order to further reveal the proposed charge transfer direction, photo-labelling experiments[51] were developed based on a fundamental fact of electrochemistry: reduction of a species is achieved at locations where electrons are trapped. The working principle of this type of experiments has been illustrated in Chapter 3 (section 3.3.3). The $RhO_x|GaNZnO$ or $RhCrO_x|GaNZnO$ system was selected to represent the $MO_x|GaNZnO$ PPC systems.

For this work, a complete photo-labelling experiment requires two steps: first, the successful photodeposition of Pt onto the PPC system (ideally either on light-absorber or on the cocatalyst); second, characterization via STEM and surface element mapping via EDS (refer Chapter 3). The first step has been detailed in chapter 3 already. The second step is critical for the charge transfer direction determination, as it provides direct visualization of the spatial distribution of the reduced Pt species on the PPC surface.

It may be worth-mention that additional imaging difficulties could be brought by too low or too high target deposition of Pt. For example, when the target loading of Pt is 0.5%, there will be little reduced Pt on surface to be distinguished from the EDS background noise; when the target loading is 5%, excess amount of the reduced Pt species appears to be homogeneously distributed on the PPC surface, disabling the spatial visualization of surface species, such as Ga, Zn, Rh, Cr, and etc.

The STEM/EDS images in Figure 4.8 are resulted from an intermediate Pt target loading (2.5%) onto a $RhO_x|GaNZnO$ PPC system.

The STEM and EDS characterization results of the sample prior to and after the photo-labelling experiment are compiled in Figure 4.8 below.
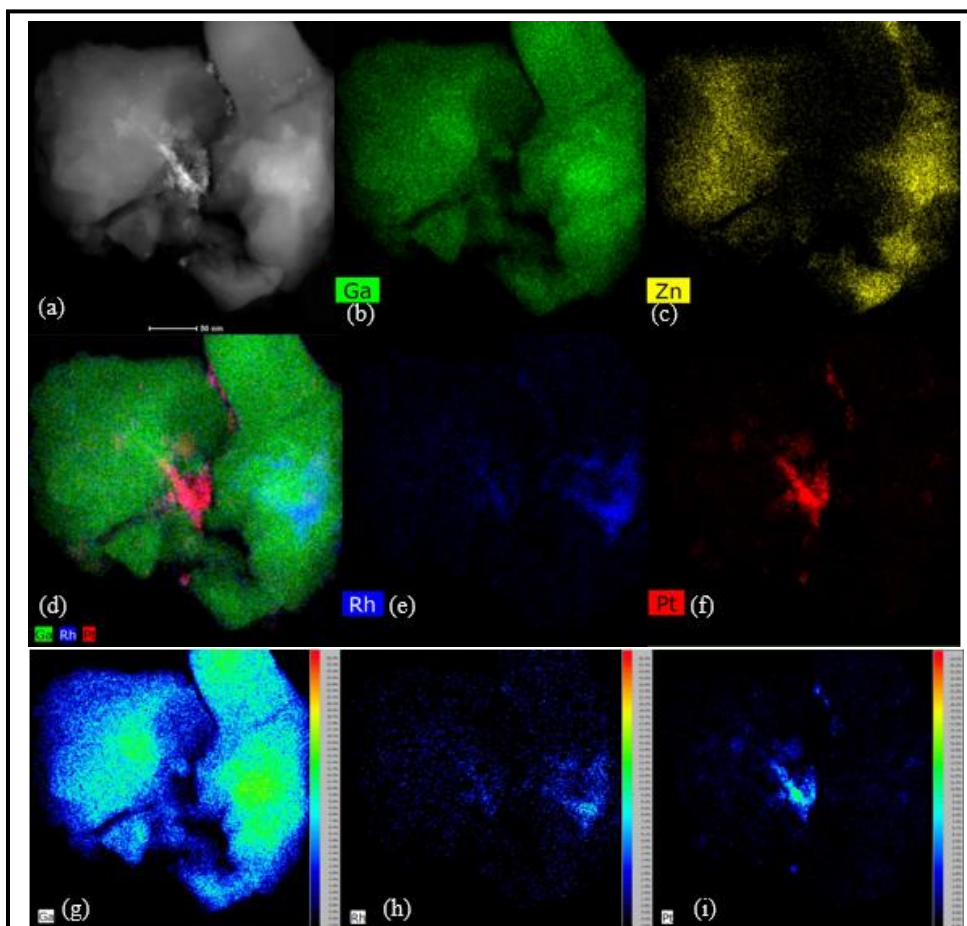
Figure 4.8 A region of negatively correlated Pt (red) and RhO_x (blue) signals, indicating photodeposition of Pt on GaNZnO surface (green, Ga as reference). (a) is HAADF image; (b), (c), (e), and (f) are surface EDS mapping of the respective elements; (d) is the superposition of element distribution on GaNZnO surface. (g)-(i) are surface composition analysis for the respective Ga, Rh, and Pt species of the region.

From the photo-labelling experiment results, a negative correlation has been established for the surface concentration between Pt and Rh species, which suggests that

reduction of Pt^{4+} to Pt mostly happened on GaNZnO surface as active electrons generated by GaNZnO are present, while photo-generated holes travel to the cocatalyst (RhO_x). The observed spatial distribution of metal elements after the photodeposition tracing experiment confirmed our hypothesis: the cocatalyst serves as the hole trap, and the n-type light-absorber serves as the electron trap during photocatalytic reaction process.

We believe this opposite-to-convention charge transfer direction also explains why oxidation half-reaction becomes more rate-limiting for OWS and HER reactions in this study. Since it has been demonstrated in both fields of photocatalytic and electrolytic water splitting where the use of metal oxides could greatly reduce the overpotential of OER[51], it is reasonable to understand that photo-generated holes become more effective when travel and initiate oxidation reaction on the metal oxides than being trapped on the surface of the light-absorber.

Such hole transfer direction from light-absorber to cocatalyst was also observed by an earlier work[51] by Townsend et al. The system being studied was $SrTiO_3$ loaded with NiO and Ni. Noticeably $SrTiO_3$ is also an n-type semiconductor[1,51].

4.4 The Revised Water Splitting Mechanism for Cocatalyst-loaded GaNZnO

Evidenced and proven by kinetics studies and photo-labelling experiments, we demonstrated that water splitting activity of cocatalyst|GaNZnO PPC systems can be kinetically improved by increasing the oxidation power of the system, as water oxidation is the initiation step of water splitting for such PPC systems. This phenomenon is confirmed by demonstrating the newly proposed movement of holes and electrons on PPC surface (Figure 4.9).

Figure 4.9 An schematic illustration of the revised redox reaction mechanism for cocatalyst|light-absorber PPCs, showing that electrons remain on GaNZnO surface, while holes can migrate to cocatalyst.
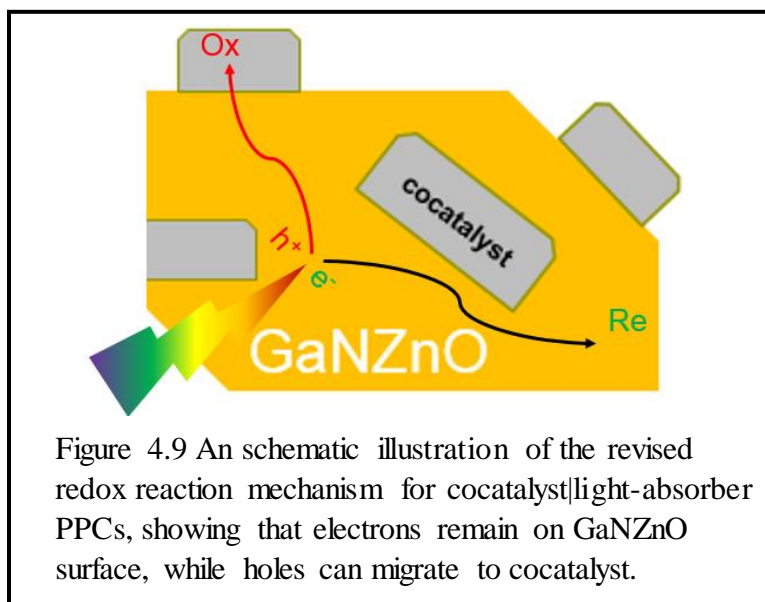
This revised mechanism thus states that holes migrate to the cocatalyst where the overpotential of oxidation half reaction could be reduced if the cocatalyst is certain types of metal oxides. The lowered overpotential for oxidation half reaction may have contributed to the RLS shift that we observe in this work.

Chapter 5. Conclusions and Future Work

5.1 Summary of Findings

Our OWS and HER study on GaNZnO further confirmed that pure water splitting and hydrogen generation from water are strongly affected by oxidation reaction involved with photo-excited holes, even though water splitting on n-type semiconductor systems is traditionally regarded to be HER limited. Photocatalytic water splitting can be limited by both reduction and/or oxidation half reactions.

By lowering the barrier of oxidation half reaction, water splitting activity can be greatly promoted with cocatalyst|n-type light-absorber PPCs. Two approaches could be useful for lowering the oxidation reaction barrier: (1) the application of more oxidizable SRs, and (2) divert photogenerated holes to desirable metal oxide cocatalysts where the overpotential of oxidation reaction can be lower than on other surfaces[51].

The band-bending phenomena have been observed for cocatalyst|GaNZnO system via the photo-labeling experiment and the accompanied STEM and EDS characterization techniques. The band-bending effect is explained by energy level re-alignment theory upon the contact of two non-identical photocatalytic materials, and can have significant impact on RLS and initiation of water splitting reaction of PPC systems.

5.2 Conclusions

The re-investigation of water splitting process by n-type light absorber confirmed that OWS needs to be initialized by oxidation half reaction. The shift in water splitting mechanism is believed to be caused by the direct interaction or contact between light-absorber and cocatalysts, which may not have been well elucidated through the macroscale electrolytic cell systems. We also expect such phenomenon to be generalized for other particulate photocatalytic systems with the classic cocatalyst|light-absorber configuration.

We also conclude that the junction formation between the light-absorber and cocatalyst can greatly influence water splitting kinetics by reversing the charge transfer direction, as revealed by the photo-labelling experiment. The reversed charge transfer direction is attributed to a band bending-up scheme caused by the interfacial junction formation.

The successful tracking of charge movements on PPCs can provide more insights to the more effective design of cocatalyst|light-absorber system for watersplitting focuses. For instance, the charge transfer direction can be manipulated by changing the interfacial electronic structures of light-absorber and cocatalyst.

5.3 Potential Future Work

The exploration of the nano-scale PPC water splitting system is still highly challenging for surface studies, such as site specific characterization. Microscopic experiments can be further explored to discover more detailed reaction and charge transfer phenomena on nano-sized photocatalyst surfaces. Those advanced microscopic methods are also expected to provide more quantifiable details to parameterize the PPC systems.

Nevertheless, water splitting via solar energy will sure become more feasible thanks to the advancement of technology, infrastructure, and societal values and demands. Thus, the prospective prevalence of photocatalytic water splitting as a sustainable hydrogen generation source will depend not only on engineering designs, but also on environmental protection awareness education and other paradigm shifts that will catalyze the switch from fossil fuel to hydrogen.

5.4 References

1. Fierro, J.; de la Mano, J. A. V.; Yerga, R. M. N.; Galván, M. C. Á.; del Valle, F. *ChemSusChem* 2009, *2*, 471–485.

2. Lewis, N. S.; Nocera, D. G. Proceedings of the National Academy of Sciences 2006, 103, 15729–15735.

3. Lanz, A.; Heffel, J.; Messer, C. *Hydrogen Fuel Cell Engines and Related Technologies*; 1st ed.; College of the Desert: Palm Desert, 2001; pp. 1-41.

4. Pilatowsky, I.; Romero, R.; Isaza, C.; Gamboa, S.; Sebastian, P.; Rivera, W. *Cogeneration Fuel Cell-Sorption Air Conditioning Systems*; 1st ed.; Springer London: London, 2011; pp. 25-35.

5. Perez, R.; Zweibel, K.; Hoff, T. E. *Energy Policy* 2011, *39*, 7290–7297.

6. Pattabathula, V.; Richardson, J. *CEP*. 2016.

7. Hydrocracking is an important source of diesel and jet fuel - Today in Energy - U.S. Energy Information Administration (EIA) https://www.eia.gov/todayinenergy/detail.php?id=9650 (accessed Mar 1, 2017).

8. Talking About Trans Fat: What You Need to Know https://www.fda.gov/Food/IngredientsPackagingLabeling/LabelingNutrition/ucm079609.htm (accessed Mar 1, 2017).

9. Gregory, D. *Scientific American* 1973, *228*, 13-21.

10. Züttel, A.; Borgschulte, A.; Schlapbach, L. *Hydrogen as a future energy carrier*; 1st ed.; Wiley: Weinheim, 2011.

11. Rutherford, A. *Trends in Biochemical Sciences* 1989, *14*, 227-232.

12. The Light-Dependent Reactions of Photosynthesis · Concepts of Biology http://philschatz.com/biology-concepts-book/contents/m45452.html (accessed Mar 1, 2017).

13. Nocera, D. *Accounts of Chemical Research* 2012, *45*, 767-776.

14. Walter, M.; Warren, E.; McKone, J.; Boettcher, S.; Mi, Q.; Santori, E.; Lewis, N. *Chemical Reviews* 2010, *110*, 6446-6473.

15. Hydrogen Production: Natural Gas Reforming | Department of Energy https://energy.gov/eere/fuelcells/hydrogen-production-natural-gas-reforming (accessed Mar 1, 2017).

16. Kreuter, W.; Hofmann, H. *International Journal of Hydrogen Energy* 1998, *23*, 661-666.

17. Boddy, P. *Journal of The Electrochemical Society* 1968, *115*, 199-203.

18. Bard, A.; Faulkner, L. *Electrochemical methods and applications*; 2nd ed.; John Wiley & Sons, Inc: New York, 2001.

19. Guo, Z.; Gong, X.; Wang, Z.; Wang, M. *Renewable and Sustainable Energy Reviews* 2014, *29*, 573-588.

20. Nowotny, J.; Sorrell, C.; Bak, T.; Sheppard, L. *Solar Energy* 2005, *78*, 593-602.

21. Honda, K.; Fujishima, A. *Nature* 1972, *238*, 37-38.

22. Linsebigler, A.; Lu, G.; Yates, J. *Chemical Reviews* **1995**, *95*, 735–758.

23. Pinaud, B.; Benck, J.; Seitz, L.; Forman, A.; Chen, Z.; Deutsch, T.; James, B.; Baum, K.; Baum, G.; Ardo, S.; Wang, H.; Miller, E.; Jaramillo, T. *Energy & Environmental Science* 2013, *6*, 1983.

24. Licht, S.; Wang, B.; Mukerji, S.; Soga, T.; Umeno, M.; Tributsch, H. *The Journal of Physical Chemistry B* 2000, *104*, 8920-8924.

25. J. M. Lehn, J. P. Sauvage, R. Ziessel, *Nouv. J. Chim.* 1980, 4, 623.

26. S. Sato, J. M. White, *Ind. Eng. Chem. Prod. Res. Dev.* 1980, 19, 542.

27. K. Domen, S. Naito, M. Suma, T. Onishi, K. Tamaura, J. *Chem. Soc. Chem. Commun.* 1980, 543.

28. Texas University at Austin Department of Chemistry. *The Design of Semiconductor Photoelectrochemical Systems for Solar Energy Conversion*; DEFENSE TECHNICAL INFORMATION CENTER: Austin, TX, 1981.

29. Darwent, J. *Journal of the Chemical Society, Faraday Transactions 2* 1981, *77*, 1703.

30. Maeda, K.; Teramura, K.; Saito, N.; Inoue, Y.; Domen, K. *Journal of Catalysis* 2006, *243*, 303-308.

31. Dare-Edwards, M.; Goodenough, J.; Hamnett, A.; Nicholson, N. *Journal of the Chemical Society, Faraday Transactions 2* 1981, *77*, 643.

32. Yoshida, M.; Takanabe, K.; Maeda, K.; Ishikawa, A.; Kubota, J.; Sakata, Y.; Ikezawa, Y.; Domen, K. *The Journal of Physical Chemistry C* 2009, *113*, 10151-10157.

33. Hashiguchi, H.; Maeda, K.; Abe, R.; Ishikawa, A.; Kubota, J.; Domen, K. *Bulletin of the Chemical Society of Japan* 2009, *82*, 401-407.

34. Carmo, M.; Fritz, D.; Mergel, J.; Stolten, D. *International Journal of Hydrogen Energy* 2013, *38*, 4901-4934.

35. Baca, A.; Ren, F.; Zolper, J.; Briggs, R.; Pearton, S. *Thin Solid Films* 1997, *308-309*, 599-606.

36. Lee, M.; Sheu, J.; Hu, C. *Applied Physics Letters* 2007, *91*, 182106.

37. Hermann, C.Sapoval, B. *The Physics of Semiconductors*; 1st ed.; Springer-Verlag New York Inc.: United States, 1995.

38. Hisatomi, T.; Maeda, K.; Takanabe, K.; Kubota, J.; Domen, K. *The Journal of Physical Chemistry C* 2009, *113*, 21458-21466.

39. Moniz, S.; Shevlin, S.; Martin, D.; Guo, Z.; Tang, J. *Energy Environ. Sci.* 2015, *8*, 731-759.

40. Uddin, M.; Nicolas, Y.; Olivier, C.; Toupance, T.; Müller, M.; Kleebe, H.; Rachut, K.; Ziegler, J.; Klein, A.; Jaegermann, W. *The Journal of Physical Chemistry C* 2013, *117*, 22098-22110.

41. Zhang, Z.; Yates, J. *Chemical Reviews* 2012, *112*, 5520–5551.

42. Maeda, K.; Hashiguchi, H.; Masuda, H.; Abe, R.; Domen, K. *The Journal of Physical Chemistry C* 2008, *112*, 3447-3452.

43. Takata, T.; Pan, C.; Domen, K. *Science and Technology of Advanced Materials* 2015, *16*, 033506.

44. Maeda, K.; Takata, T.; Hara, M.; Saito, N.; Inoue, Y.; Kobayashi, H.; Domen, K. *Journal of the American Chemical Society* 2005, *127*, 8286-8287.

45. Yashima, M.; Maeda, K.; Teramura, K.; Takata, T.; Domen, K. *Chemical Physics Letters* **2005**, *416*, 225–228.

46. Hashiguchi, H.; Maeda, K.; Abe, R.; Ishikawa, A.; Kubota, J.; Domen, K. *Bulletin of the Chemical Society of Japan* **2009**, *82*, 401–407.

47. Maeda, K; Teramura, K; Domen, K. *Journal of Catalysis* **2008**, *254*, 198–204.

48. Trasatti, S. *Electroanalytical Chemistry and Interfacial Electrochemistry* **1972**, *39*, 163–182.

49. Maeda, K.; Teramura, K.; Lu, D.; Takata, T.; Saito, N.; Inoue, Y.; Domen, K. *Nature* **2006**, *440*, 295–295.

50. Matsubu, J.; Lin, E.; Gunther, K.; Bozhilov, K.; Jiang, Y.; Christopher, P. *Catal. Sci. Technol.* 2016, *6*, 6836-6844.

51. Townsend, T.; Browning, N.; Osterloh, F. *Energy & Environmental Science* 2012, *5*, 9543.

52. Hecht, H. *Journal of Research of the National Bureau of Standards Section A: Physics and Chemistry* 1976, *80A*, 567.

53. Ikeda, S.; Takata, T.; Komoda, M.; Hara, M.; Kondo, J.; Domen, K.; Tanaka, A.; Hosono, H.; Kawazoe, H. *Physical Chemistry Chemical Physics* 1999, *1*, 4485-4491.

54. Maeda, K.; Domen, K. *The Journal of Physical Chemistry Letters* 2010, *1*, 2655-2661.

55. Haynes, W.; Lide, D. *CRC handbook of chemistry and physics*; 93rd ed.; CRC Press: Boca Raton, Fla. [u.a.], 2012.

56. Reber, J.; Meier, K. *The Journal of Physical Chemistry* 1984, *88*, 5903-5913.

57. Xu, Y.; Schoonen, M. *American Mineralogist* 2000, *85*, 543-556.

58. Schneider, J.; Bahnemann, D. *The Journal of Physical Chemistry Letters* 2013, *4*, 3479-3483.

59. Kawai, T.; Sakata, T. *Journal of the Chemical Society, Chemical Communications* 1980, 694.

60. Chakrabarti, S.; Chaudhuri, B.; Bhattacharjee, S.; Ray, A.; Dutta, B. *Chemical Engineering Journal* 2009, *153*, 86-93.

61. Buehler, N.; Meier, K.; Reber, J. *The Journal of Physical Chemistry* 1984, *88*, 3261-3268.

62. Heiskanen, A.; Yakovleva, J.; Spégel, C.; Taboryski, R.; Koudelka-Hep, M.; Emnéus, J.; Ruzgas, T. *Electrochemistry Communications* 2004, *6*, 219-224.

63. Maeda, K.; Teramura, K.; Masuda, H.; Takata, T.; Saito, N.; Inoue, Y.; Domen, K. *The Journal of Physical Chemistry B* 2006, *110*, 13107-13112.

64. McCrory, C.; Jung, S.; Ferrer, I.; Chatman, S.; Peters, J.; Jaramillo, T. *J. Am. Chem. Soc* 2017, *137*, 4347-4357.

65. Yoshimura, J.; Ebina, Y.; Kondo, J.; Domen, K.; Tanaka, A. *The Journal of Physical Chemistry* 1993, *97*, 1970-1973.

66. Roy, A.; SASMAL, G.; BHATTACHARYYA, S. *International Journal of Hydrogen Energy* 1995, *20*, 627-630.